Investigation of High Resolution 3D Rodent-morphic Dosimetry, and Cost-Effective Optical-CT using Fresnel Lenses

by

Steven Terrance Bache

Graduate Program in Medical Physics
Duke University

Date:

Approved:

_____
Mark Oldham, Supervisor

_____
Shiva Das

_____
Martin Tornai

Thesis submitted in partial fulfillment of
the requirements for the degree of Master of Science in
the Graduate Program in Medical Physics in
the Graduate School of
Duke University

2014

ABSTRACT

Investigation of High Resolution 3D Rodent-morphic Dosimetry, and Cost-Effective

Optical-CT using Fresnel Lenses

by

Steven Terrance Bache

Graduate Program in Medical Physics
Duke University

Date:

Approved:

_____
Mark Oldham, Supervisor

_____
Shiva Das

_____
Martin Tornai

An abstract of a thesis submitted in partial fulfillment of
the requirements for the degree of Master of Science in
the Graduate Program in Medical Physics in
the Graduate School of
Duke University

2014

Abstract

Micro-irradiators enable exploration of the efficacy of novel radiation treatment approaches by providing the capability to reproduce realistic treatment delivery in small animal models. An approach of current topical interest is hypofractionated stereotactic body radiation therapy (SBRT), and the study of associated tumor and normal tissue radio-biology. Rodent SBRT is extremely challenging, requiring the precise delivery of radiation beams on the order of several millimeters. At present there are no methods to comprehensively verify these delivery techniques due to the requirements for ultra-high resolution and ability to measure the dose in 3 dimensions (3D).

This work introduces a potential solution to the rodent SBRT verification challenge: radiochromic rodent-morphic 3D dosimeters compatible with ultra-high resolution optical computed tomography (optical-CT) dose read-out. Rodent-morphic dosimeters were produced by 3D-printing molds of rodent anatomy directly from X-ray CT data, and using these molds to create tissue-equivalent phantoms both with and without high-Z spinal inserts for cone-beam CT targeting. Feasibility was evaluated through a series of irradiations, including a 180-degree spinal arc treatment. Dose distributions were measured in high-resolution (0.5mm isotropic voxels) with an in-house built optical-CT system, which determined dose from the change in optical density throughout the dosimeters from pre-and post-irradiation scans. Optical-CT data

was calibrated to absolute dose using a calibration curve determined from irradiating small volumes of radiochromic material from the same batch as the rodent-morphic dosimeters to known doses in a 6MV beam (negligible energy response was assumed). Independent verification of absolute dose at a point was made with a novel scintillator comprised of europium and lithium doped yttrium oxide nanocrystals, with a sub-mm active length. Independent verification of the dose distribution was performed using EBT2 radiochromic film positioned in the dosimeters, which had been sliced in half. Contrast-to-noise ratio between high-Z spinal inserts and tissue-equivalent PRESAGE material was found to be ~10, sufficient for bony alignment and isocenter targeting with on-board CBCT image guidance. Absolute dose calculated at isocenter through optical-CT was found to agree with nano-detector measurement within 3%, while relative dose distributions in two orthogonal planes were found to agree with film within 4%. PRESAGE rodent-morphic dosimeters demonstrated much promise in the verification of precise radiation treatment given by the X-Rad 225Cx micro-irradiator.

Practical challenges involved in optical-CT imaging were addressed through the investigation of an in-house Fresnel-based optical-CT system with considerably less refractive index-matching fluid. The "DFOS" (Duke Fresnel-based Optical-CT System) system differed from current optical-CT systems by replacing cumbersome convex telecentric lenses with a lighter and much less expensive Fresnel system. A second major modification was the replacement of the refractive index-matching fluid bath with

a solid polyurethane tank. PRESAGE radiochromic dosimeters were irradiated with orthogonal parallel-opposed treatments and a brain IMRT treatment and dose distributions were readout by the DFOS system and compared to both treatment planning software prediction and other in-house optical-CT systems. Gamma index passing rate at the 3%/3mm threshold for the two parallel-opposed and brain IMRT treatments were 89.3%, 92.1%, and 87.5%, respectively. The DFOS system showed promise for 3D dosimetry, but the performance is still substantially inferior at present to the gold-standard systems.

Contents

List of Tables

List of Figures

Acknowledgements

I would like to thank the following people their time, assistance, and support:

Thesis Committee

Mark Oldham, PhD – Advisor (thanks!)

Shiva Das, PhD

Martin Tornai, PhD

Duke 3D Dosimetry and Bio-Imaging Lab

Titania Juang

Jake Jackson

Qiongge Li

Kelsey Chisolm

Javian Malcolm

Leith Rankine

Don Pearce – Duke machine shop

Small Animal Irradiator

David Kirsch, PhD

Hooney Minn

Matt Belley

Hannah Norris

Rider University

John Adamovics, PhD

Ron Benning

Lastly, and most importantly- thank you Gretchen Leigh Guggenheim for staying by my side, and for agreeing to marry me *after* Graduate School!

This work was partially supported by NIH R01CA100835.

1. Introduction

1.1 Small Animal Irradiation Research

The current assumption in radiation treatment for cancer is that the most effective way to treat a region of cancerous cells is to irradiate the entire volume with as high a dose as possible while sparing normal tissue. In recent years, however, the ability to investigate complex radiation deliveries and associated radio-response has been made possible through small animal radiation research platforms[1-6]. This pre-clinical setting is important for exploring tumor radio-response in small animal tumor models. Small animal micro-irradiators such as the X-Rad 225Cx (Precision X-Ray, N. Banfield, CT) allow precise, image-guided treatment to small animals (e.g. rats or mice) with field sizes as small as 10x10 mm^2. Investigations of tumor response in differing radiation treatment courses such as extreme hypo-fractionation and partial-tumor irradiation have become possible in this pre-clinical small animal setting. This is similar to early phase clinical trials of new drugs, where rodent studies are completed before translating to human populations.

It is important to note that this pre-clinical radiotherapy setting should not only be scaled down in geometry, but also in energy. The use of MV beams in small animal radiotherapy is ill advised due to dose buildup regions at the specimen surface, as well as field penumbra with sizes on the order of the entire specimen itself. The use of kV

beams (225 kVp for the X-Rad225Cx) introduces the challenge of high-resolution treatment planning and verification, where commercial treatment planning software is inaccurate.

Investigation into high-resolution treatment planning and dose verification is necessary. Software utilizing Monte-Carlo simulation and superposition convolution methods are of current interest for small animal treatment planning[7-10]. In this work, the challenge of measuring high-resolution 3D dose distributions given by a small animal micro-irradiator is addressed. High-resolution, rodent-morphic PRESAGE dosimeters were produced, with 3D dose readout accomplished through the use of optical-CT. This section is organized as follows: Chapter 2 contains a brief description of the custom optical-CT readout system available in the Duke University 3D dosimetry and bio-imaging lab, as well as the radio-response characteristics of PRESAGE radiochromic dosimeters (Hueris Pharma, Skillman, NJ). Chapter 3 introduces a series of novel rodent-morphic PRESAGE dosimeters produced through 3D printing of rodent molds directly from CT data. The rodent-morphic dosimeters were developed for use in imaging high-resolution 3D dose distributions given by the X-Rad 225Cx small animal irradiator at Duke. Quantitative analysis of a rodent stereotactic body radiation therapy (SBRT) treatment delivered to a rodent-morphic phantom is discussed.

1.2 Convenient, Cost-effective Optical-CT

Chapter 4 describes an investigation into the feasibility of a more convenient and cost-effective "dry" optical-CT scanner. This "DFOS" (Duke Fresnel-based Optical-CT System) attempts to address two difficulties associated with optical-CT scanning. It utilizes: (1) a telecentric Fresnel lens system, reducing weight and cost compared to standard convex telecentric lenses and (2) a polyurethane tank for minimizing the amount of refractive-index matching fluid needed to read out high-resolution 3D dose distributions in PRESAGE radiochromic dosimeters.

2. 3D Dosimetry with Optical Computed Tomography

Several materials and methods for imaging 3D dose distributions have been proposed and utilized. Gels doped with an aqueous ferrous sulfate solution (Fricke gels) allow both MR and optical readout of dose distributions[11, 12]. Fricke gel dosimetry works through the dose dependent transformation of ferrous ions (Fe^{2+}) to ferric ions (Fe^{3+}), which causes a paramagnetic shift observable with MRI[13]. Resolution is limited in Fricke gels due to the diffusion of ferric ions post-irradiation blurring the dose distribution. Similarly, polymer gels display a change in opacity upon irradiation due to a dose dependent polymerization within the gel[14, 15]. Imaging of opacity change in polymer gels, and therefore dose, through optical-CT relies on the differential scattering of incident visible light. The scattering from polymers is not ideally localized, which can also blur the 3D dose distribution[16]. For highly localized and thus high-resolution 3D dosimetry, dose-dependent differential light *absorbance* is an attractive alternative to both paramagnetic changes and optical scattering.

2.1 PRESAGE radiochromic dosimeters

PRESAGE dosimeters consist of an optically clear polyurethane matrix doped with a radiochromic leuco-dye[17]. The leuco-dye, leucomalachite green (LMG), changes light absorbance when exposed to ionizing radiation, which can be quantified as a change in optical density. The advantage of differential absorbance upon irradiation is

the truly local nature of the dose-dependent change in the dosimeter. PRESAGE characteristics have been well documented to show a linear change in optical density with respect to absorbed dose that is dose-rate and energy independent[18, 19]. PRESAGE is also insensitive to oxygen and visible light, and can be cast and cured in a variety of shapes. PRESAGE material is generally made to be tissue equivalent, but the effective atomic number may be changed by altering the relative proportions of leuco-dye and initiator[20] used in production. A further benefit of PRESAGE optical dose readout is the ability to deliver dose treatments to moving or deformed[21] phantoms, mimicking difficult planning and verification scenarios seen in the clinic. Readout of dose distributions in PRESAGE dosimeters is accomplished through optical-CT, described in the next section. Examples of past usage of PRESAGE 3D dosimetry include head and neck treatment verification[22], as well as the commissioning[23] and image-guidance verification[24] for the X-Rad 225Cx small animal irradiator at Duke University.

2.2 Optical Computed Tomography

Optical computed tomography, or optical-CT, was first introduced in 1996 for imaging dose distributions in polymer gels[25], and is the visible light analogue to first-generation X-ray CT. For this work, in-house optical-CT systems of differing scales were used for all imaging. Some features of each system referenced in this paper are listed in Table 1.

Table 1 – Specifications of in-house optical-CT systems available in the Duke 3D Dosimetry and Bio-Imaging Lab

System Name (Duke <size> Optical-CT System)	Lens Diameter [cm]	Matching-fluid necessary [cc]	CCD	Pixel Size [microns/px]	Reconstructed voxel size (typical) [mm]
DLOS < Large >	30	13500	Basler A1021	6.45	1-2
DMOS < Mid-sized>	17	3240	Basler A1021	7.4	0.5
DmicrOS < Micron >	7	216	Basler pIA1600-35gm	6.45	0.05-0.1
DFOS < Fresnel-based >	24	100	Basler pIA1600-35gm	7.4	1-2

Figure 1 shows a schematic of the Duke Large FOV Optical–CT System (DLOS) first described in Thomas et al[26] in 2010 and benchmarked in 2011[27]. To obtain volumetric dose data within the dosimeter, a sample is immersed in a refractive index-matching bath and placed on a stage within the FOV of a matched telecentric source and imaging lens (Edmund Optics, Barrington, NJ). The fluid minimizes deviation from parallel beam incidence at the sample interfaces by eliminating refractive index mismatching (further discussion in Chapter 4). An LED with peak output at 632nm and +/- 10nm filter (to match peak PRESAGE response) is collimated into parallel-beam geometry and used to illuminate the sample. Typically 360 projections of differentially

attenuating line paths are made at 1-degree increments and captured after collimation by a CCD array (Basler, Germany).

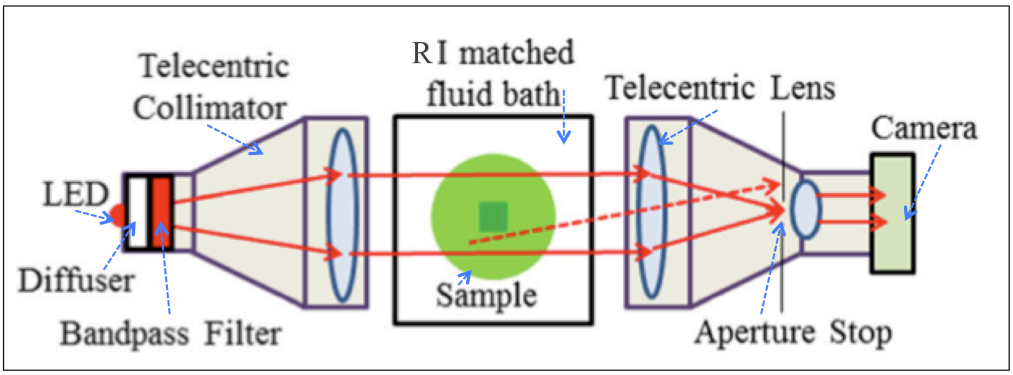

Figure 1 - Schematic of DLOS optical-CT System (Image courtesy of Andy Thomas, PhD)

The quantity of interest in optical-CT with PRESAGE is the change in optical density throughout the volume upon irradiation, which is defined as $-\log_{10}\left[\frac{I}{I_o}\right]$, where I_0 is the incident optical intensity and I is the intensity through the sample. To reconstruct optical density change throughout the volume, intensity projections through the sample must be made both pre- and post-irradiation, as well as initial intensity projections. Initial intensity I_0 is measured both pre- and post-irradiation through a "flood" field – a projection through the refractive index-matching fluid filled tank without the dosimeter emerged. The flood field is discussed further in Chapter 4

3D reconstructions of optical density change in PRESAGE dosimeters are made through filtered back-projection with a custom MATLAB (MathWorks, Natick, MA) GUI

in high-resolution (up to 0.5mm isotropic) voxels. Figure 2 shows a representative pre- and post- irradiation projection, as well as a reconstructed axial slice from a 5-beam anterior-posterior treatment.

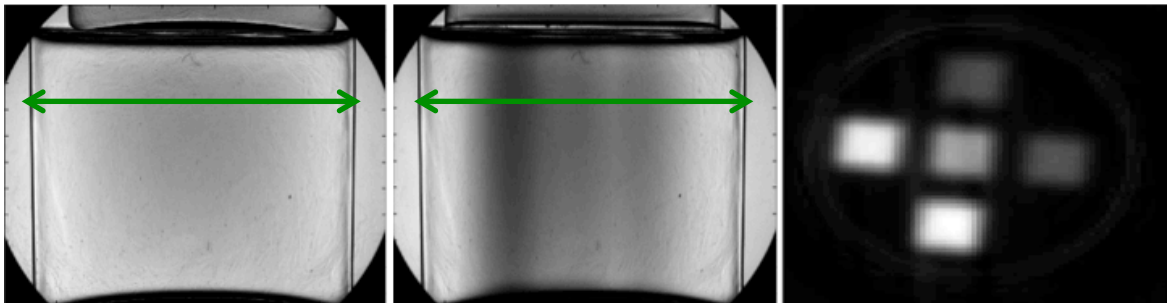

Figure 2 – Example of optical-CT projection images pre-irradiation (left), post-irradiation (center) and axial reconstructed slice (right- position in dosimeter shown with solid green arrows).

3. Rodent-morphic Dosimetry

3.1 Motivation

For the geometry and scales of clinical radiation treatment, a cylindrical dosimeter is adequate for comparing dose distributions calculated with PRESAGE and optical-CT with predicted distributions given by treatment planning software such as Eclipse [Varian Medical Systems, Palo Alto, CA]. For dosimetric considerations in the small animal setting, however, a more precise dosimeter design is desired.

In recent years, much effort has been given to the development of precise, image-guided small animal irradiators for complex radiotherapy treatment in small animal tumor models. Investigation of the efficacy and biological radio-response from new radiation treatments rely on the use of these small animal models before reaching the clinic. Pre-clinical studies aim to highlight the biological mechanisms governing radiotherapy response in many radiation applications[2-4, 28].

With more complex radiotherapy techniques being investigated comes a need for a high-resolution 3D measurement of dose distributions given by small animal micro-irradiators such as the X-Rad225Cx. Current practice in small animal dosimetry rely on film or TLD measurements of radiation output of small field therapy machines at acceptance and commissioning in the form of tabulated percent-depth-dose (PDD) curves, with beam-on-time for a specified delivered dose calculated from these lookup

tables. A high-resolution, 3D dose readout is desired for radiotherapy treatments given my small animal irradiators, as well as for verification of treatment planning software, which is becoming more widely available.

For this investigation, high-resolution rodent-morphic PRESAGE dosimeters were produced utilizing 3D printing of rodent anatomy directly from CT data. These anatomically accurate dosimeters were produced in order to mimic exact rodent contours and internal structures, for dose readout with high-resolution optical-CT.

3.2 Production of anatomically-correct rodent-morphic dosimeters

Evaluation of the rodent-morphic dosimeters involved (a) establishing the feasibility of manufacture both with and without high-Z heterogeneous inserts (such as bone), (b) verification of sufficient bony/soft-tissue contrast for representative CBCT image-guided positioning, and (c) achievability of relative dose-readout by optical-CT in high resolution (0.5mm isotropic voxels), with absolute dose verification at isocenter. The general workflow for producing rodent-morphic dosimeters involved (1) obtaining a CT of the rodent of interest, (2) conversion of rodent CT data to 3D-printable file format[29], (3) 3D-printing positive molds of anatomically correct outer contours and spinal inserts, and (4) using the positive molds to produce tissue equivalent PRESAGE dosimeters with high-Z PRESAGE bony inserts. The specifics of this workflow are detailed below and show in Figure 3.

3.2.1 Step 1: CT Data

For this study, a research rat was scanned following IACUC protocols with a LightSpeed RT (GE Healthcare, UK) CT system at Duke University Medical Center Clinic at 80 kVp and 75 mAs. Volumetric CT data was exported as .625 mm axial slices in DICOM (.dcm) format, and imported into 3D Slicer (www.Slicer.org), an open-source software package for visualization and image analysis[30].

3.2.2 Step 2: 3D Modeling and Post-Processing

The 3D Slicer software gives the ability to contour structures and convert and export in stereolithography (.stl) file format. For this study, a central 40.1 mm axial portion of the rat was selected, corresponding to the prostate region plus 25 mm and 5 mm margins in the superior and inferior directions respectively. Both external body and spinal contours were drawn in 3D Slicer and saved as individual structures, first with automated Hounsfield units segmentation, then refined manually. Finer details outside of the vertebral bodies were omitted. A base with thickness 1.875 mm (3 slices) corresponding to the outer contours of the rat was added to the spinal insert. This allowed precise placement of the spine within the rat body by aligning the spinal insert base with the outer body base.

After segmentation, 3D-mesh files for rat spinal and outer body contours were imported into the Meshlab (stylized meshlab, sourceforge.meshlab.net) software package, an open-source package for editing and processing 3D triangular meshes. Additional post processing was performed in meshlab in order to repair and smooth the 3D files, including 3 Laplacian smoothing iterations, and deletion of any isolated volumes smaller than 5% of the maximum mesh volume. Smoothing was done to simplify the 3D printing as well as dosimeter manufacturing steps, while isolated volume deletion ensures the absence of any structures too small to be produced in the slice-by-slice manner used by the 3D printer.

3.2.3 Step 3: 3D Printing

Smoothed and processed spine and body .stl files were sent to be 3D printed by FineLine Prototyping (Raleigh, NC), via additive manufacturing, the process of building a model slice-by-slice from the bottom up using thin layers of rapidly cooling liquid plastics. Anatomical molds were printed in 0.1 mm slices from liquid DSM Somos ProtoGen 18420, a plastic-like photopolymer[31], with 0.23 mm resolution in each in-slice dimension. These molds served as the positive molds used in the production of the PRESAGE rodent-morphic dosimeters.

3.2.4 Step 4: PRESAGE Rodent-morphic Dosimeters

3D rodent-morphic dosimeters were produced from 3D-printed molds in a 3-step process: First, a flexible, removable mold was constructed from the 3D printed spinal mold. High-Z PRESAGE material was poured and cured to produce a radio-chromic spinal insert with near-bone equivalent attenuation. A spinal base ensured proper alignment of the spine with respect to the outer body contours. Next, a similar mold was produced using the 3D printed body. The spinal insert was placed into the body mold, and lower-Z (tissue equivalent) PRESAGE material was poured into the mold and cured. This resulted in a PRESAGE radiochromic dosimeter, with outer contours and high-Z spinal insert derived directly from rat CT data.

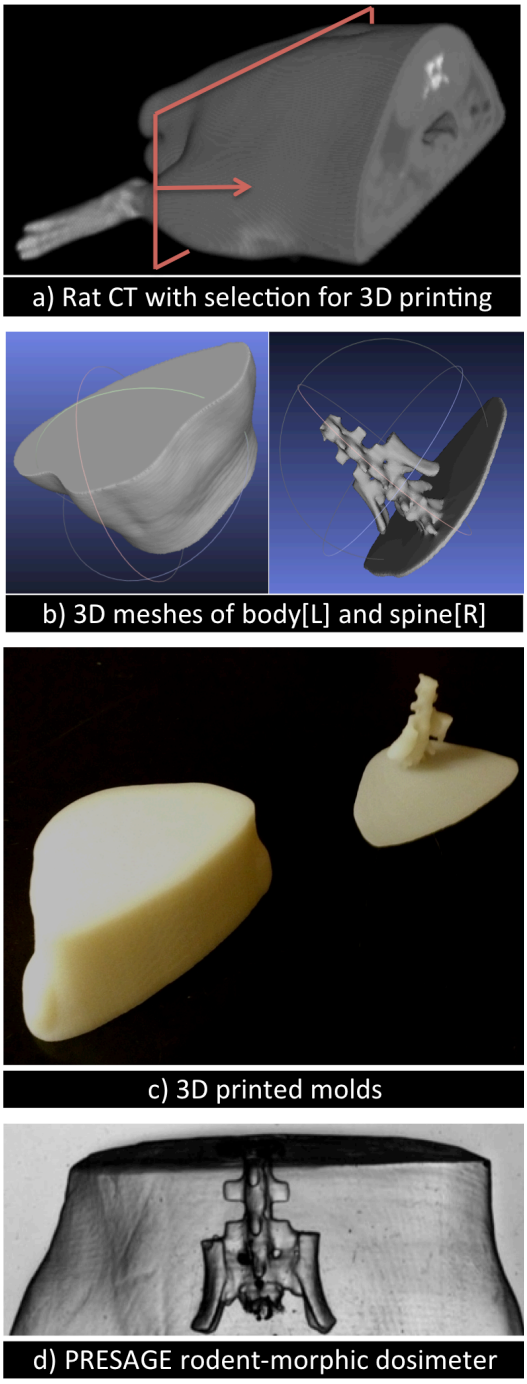

Figure 3 – Illustration of workflow for producing rodent-morphic dosimeters from CT data. Rodent CT data (a) is converted to 3D meshes (b) for printing 3D positive molds (c), which are used to make negative molds for constructing PRESAGE dosimeters (d – optical-CT projection shown to highlight spinal insert).

3.3 Treatment plans for rodent-morphic dosimeters

Several treatments were designed and delivered for the investigation of PRESAGE rodent-morphic dosimeters. An initial rat prostate treatment served as a pilot study to investigate the feasibility of manufacturing the dosimeters. (Section 3.3.1) In-depth quantitative analysis was performed with a spinal-arc micro- SBRT treatment (Section 3.3.2), and an ongoing "marginal-miss" treatment paradigm is being investigated in a mouse version of the rodent-morphic dosimeter (Section 3.3.3).

3.3.1 Rat prostate treatment

To investigate CBCT image-guidance and optical-CT readout, a simple 5-field coplanar treatment was designed. A rodent dosimeter with high-Z spinal insert was placed on the X-Rad 225Cx treatment stage and a CBCT was performed. Sufficient contrast was realized between the tissue equivalent PRESAGE and the spinal insert, and isocenter was placed 1cm to the spine. The phantom was irradiated with 5- 2.5mm diameter circular fields. Optical density change was read out using an in-house Optical-CT system analogous to the DLOS to feature a smaller FOV of 17cm x 17cm. The Duke Mid-Sized Optical-CT System (DMOS) was used to take 360 pre- and post- irradiation projection images at 1-degree increments, and optical density change was reconstructed with 0.5mm isotropic voxels. Qualitative evaluation of reconstruction edge artifacts and

isocentric beam convergence showed viability of the dosimeters. Figure 4 shows proper isocentric beam alignment and minimal edge artifacts.

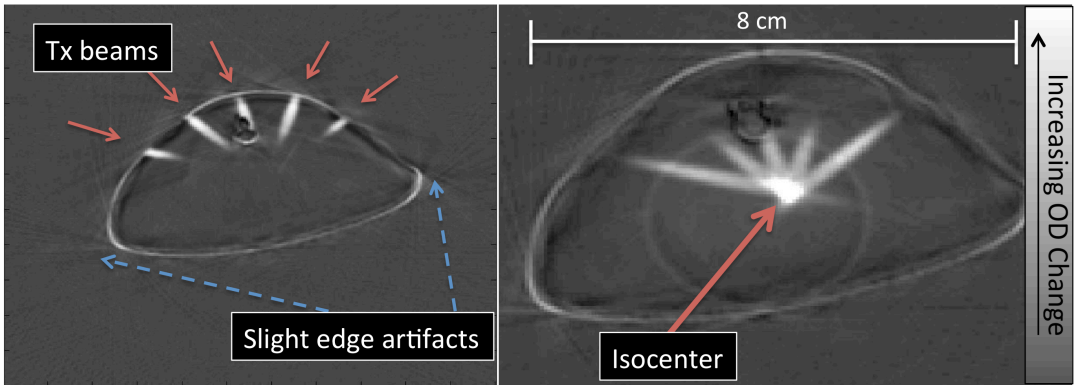

Figure 4 – Reconstructed optical-density change with 0.5mm isotropic voxels. Five incident coplanar beams are shown to converge at isocenter (solid red arrows). Slight edge artifacts are noticeable (dashed blue arrows).

3.3.2 Spinal arc treatment

For a more quantitative investigation, a treatment plan was devised in order to simulate micro-SBRT (stereotactic body radiation therapy) spinal cord treatments given by a 180-degree arc. Accurate delivery to the rodent spine was accomplished using two rodent-morphic dosimeters- an "imaging" phantom that included the high-Z spinal insert for target alignment and isocenter placement, and a homogeneous "dosimetric" phantom for dose distribution readout. The imaging phantom was first placed on the carbon fiber treatment stage in a cardboard setup-jig. To achieve accurate spinal targeting, CBCT was performed on the imaging phantom and isocenter was placed

directly on the spine. The imaging phantom was then replaced on the treatment stage by the dosimetric phantom, preserving isocenter placement. Outer contours images were overlaid and compared in order to confirm exact replacement of the imaging phantom with the homogeneous dosimetric phantom [Figure 5]. A 2 cm (AP) x 1 cm rectangular cone was selected for treatment. A 3mm lead-block (~4 HVLs) was constructed and affixed to the treatment cone to divide the 2 cm longitudinal field into a 1cm section and a 3mm section at isocenter [Figure 6]. The dosimeter was then treated in the supine position with a 180-degree arc at 225 kVp and 13 mAs, through the carbon fiber treatment stage.

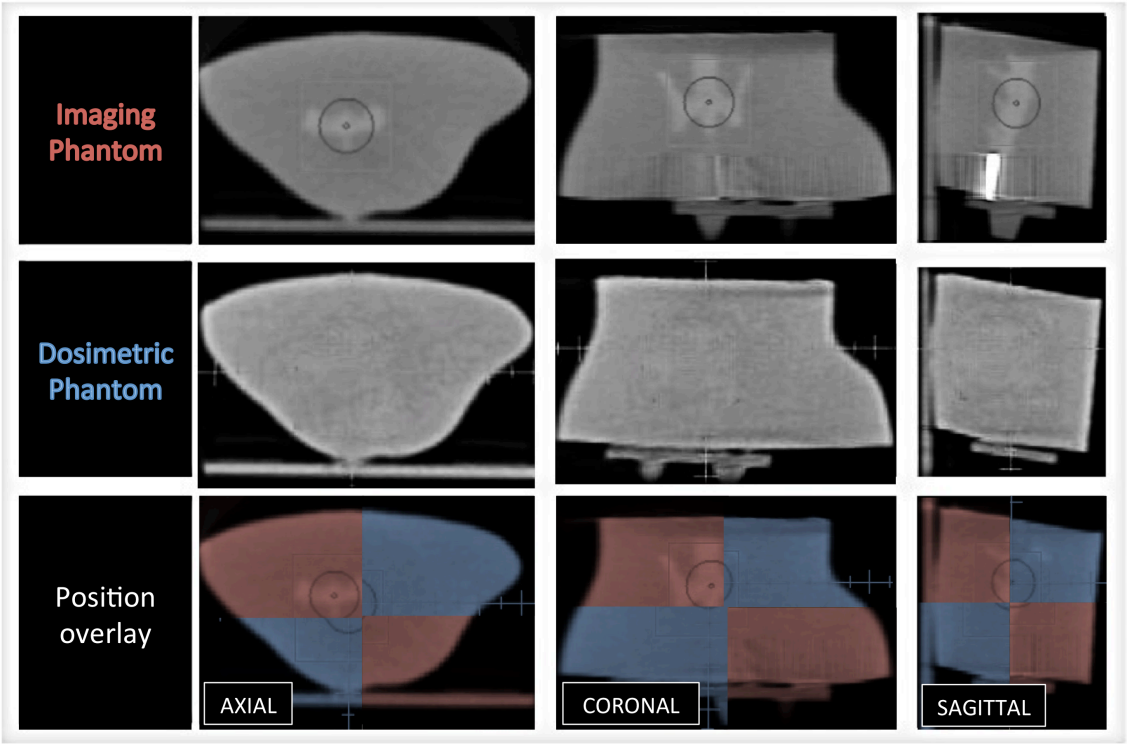

Figure 5 – CBCT of imaging (top row) and dosimetric (middle row) phantom in three orthogonal views. Proper alignment can be seen in all three views with phantom images overlaid (bottom row). The high-Z spinal insert is visible in the imaging phantom, allowing isocenter targeting. ***Some artifacts remain – Top Right: The high attenuation (bright white) artifact is produced by a small piece of metal remaining in the dosimeter from production. Imaging and isocenter placement is unaffected. Bottom Row: The rings in the center are misaligned due to the images being taken*** **before** ***isocenter adjustment.***

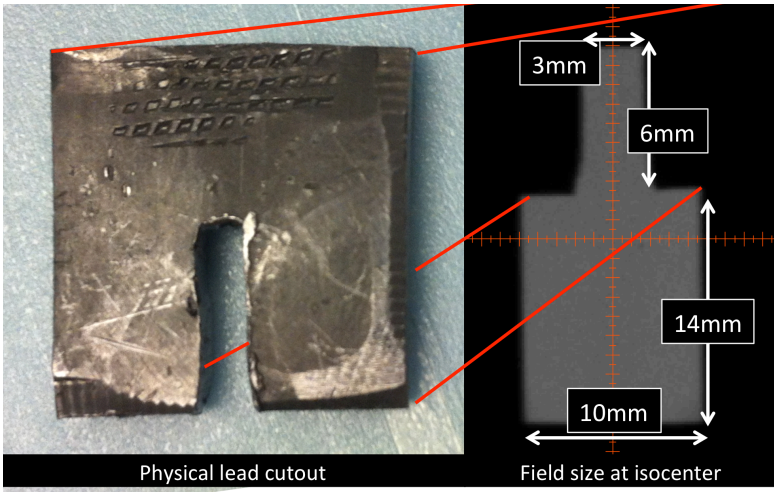

Figure 6 – Lead block (~3mm thick) cutout (left) used to divide radiation field into large and small regions, along cone-beam projection image of actual radiation field at isocenter (right).

3.3.2.1 Optical-CT readout

Optical density change was computed from 360 projection images at 1-degree increments by the DMOS system, and reconstructed with 0.5mm isotropic voxels. In order to calibrate PRESAGE sensitivity, 8- 1cm x 1cm plastic "cuvettes" consisting of PRESAGE material from the same batch used for the rodent-morphic dosimeters were analyzed. Initial optical density at 633 nm was measured for each cuvette with a Genesys 20 spectrophotometer (Thermo Spectronic, Waltham, MA), followed by an irradiation of the cuvettes by a clinical LINAC to 1Gy, 1Gy, 3Gy, 3Gy, 6Gy, and 6Gy (with two controls). Sensitivity of the rodent-morphic dosimeters in ΔOD/Gy-cm was found from a linear fit of cuvette data [Figure 7].

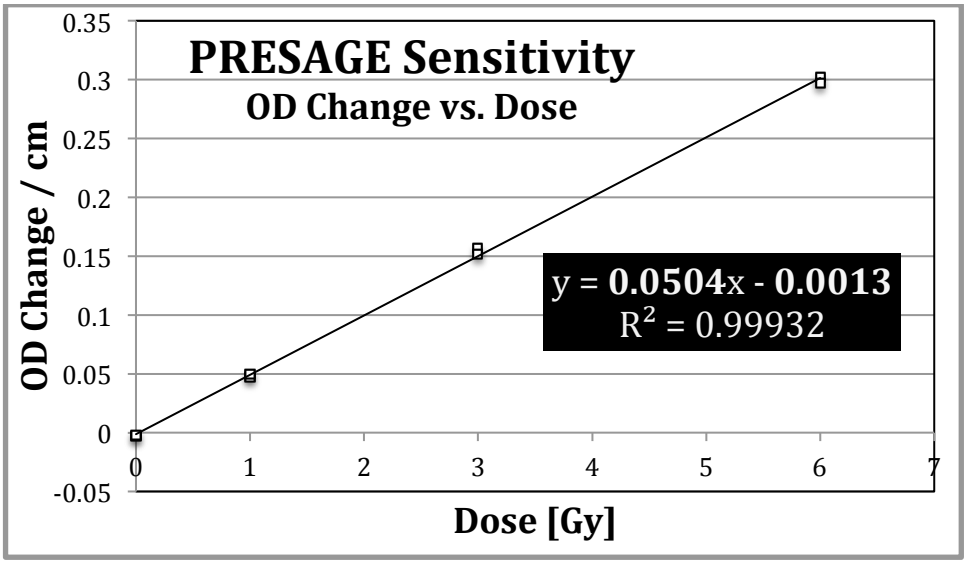

Figure 7 – Rodent-morphic PRESAGE sensitivity in [Δ OD/Gy-cm] determined from cuvette data. Formulation: o-Meo LMG 1.5%

3.3.2.2 Absolute Dose measurement

Reconstructed voxel values in OD change were converted to dose through the strong linear relationship between PRESAGE OD change and absorbed dose (R^2 = 0.99932). A cube ROI with 3 voxel (1.5mm) length sides was centered about the arc isocenter to account for any setup error, and mean isocenter dose was found to be 9.23 Gy with a 0.093 Gy standard deviation. To verify the accuracy of the PRESAGE dose distribution, two measurements were made. First, a 1mm channel was drilled into the original treated PRESAGE dosimeter. NanoFOD (nano- fiber-optic detector), a novel europium and lithium doped yttrium oxide nanocrystal-based scintillation detector[32] was used to confirm absolute dose at isocenter [Figure 8]. The 400-micron active region of the detector was calibrated in units of integrated voltage (V-s) vs. exposure (mR)

using a 0.18cc RadCal ion chamber through a series of 9 30-second open-field irradiations with the X-rad 225Cx irradiator – 3 each at 8, 10, and 13 mAs. NanoFOD calibration factor was converted from V-s/mR to soft-tissue dose in V-s/cGy using the ICRU-44 formulation, and found to be 0.235 V-s/cGy. The detector was then placed inside the PRESAGE channel after setup on the X-Rad225Cx treatment stage [Figure 8]. The original 180-degree arc treatment was repeated 3 times with the active region of the detector at treatment isocenter. The average converted tissue (and PRESAGE) dose to isocenter was found to be of 9.49 Gy (standard deviation = 0.0085 Gy), an absolute dose difference less than 3% compared to optical density measurement of 9.23 Gy.

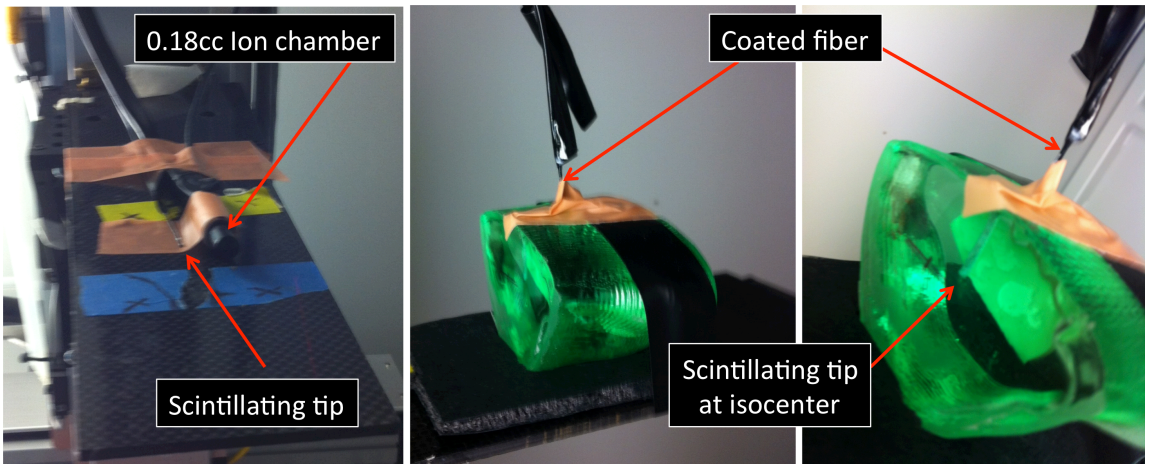

Figure 8 – Setup for absolute dose measurement at isocenter with a novel nano-scintillation detector. First, the detector was calibrated with a RadCal 0.18cc ion chamber (left), then the 180-degree arc treatment was delivered three times with the scintillating detector placed at the rodent-morphic dosimeter isocenter (center, right).

A second independent verification of dose was made with Gafchromic EBT2 radiochromic film (Ashland, Covington, KY). The radiochromic film was calibrated (units of intensity loss/Gy) by irradiating several small pieces of film from the same batch to known doses with a 6MV treatment beam (energy dependence assumed negligible), and comparing counts both pre- and post- irradiation through an Expression 10000 XL film scanner (Epson, Nagano, Japan). Square ROIs were drawn on each film slice, and average intensity loss was plotted vs. dose, and fitted with a high-dose and low-dose quadratic fit [Figure 9].

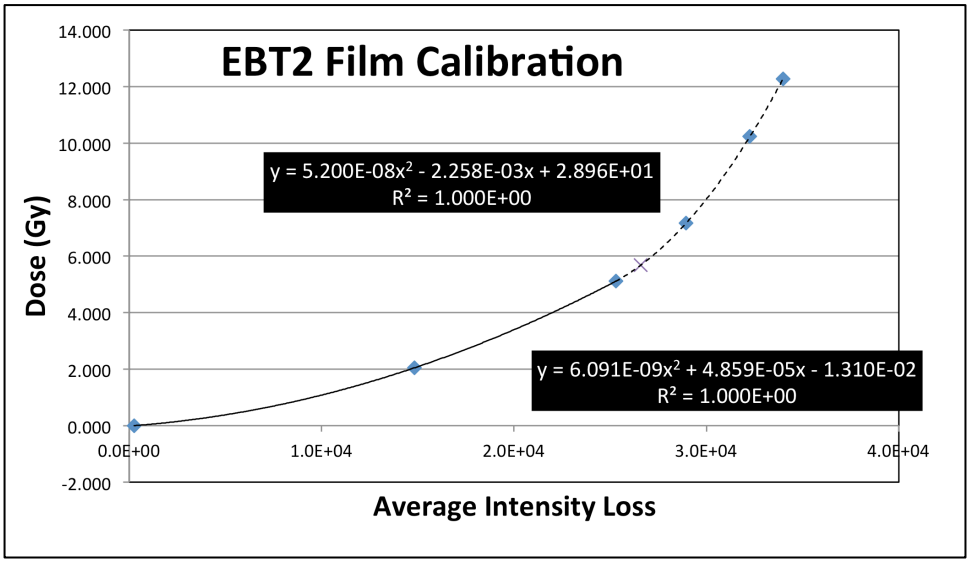

Figure 9 - Bi-quadratic fit of radiochromic film used for absolute dose verification.

In order to verify dose distributions in two orthogonal planes, the imaging and dosimetric phantoms were both machined in half at isocenter in the coronal and axial dimensions (1 each). Film was placed between the two halves and the 180-degree arc treatment was repeated for each dosimeter [Figure 10]. To measure absolute dose distributions in the axial and coronal film slices inserted into PRESAGE, intensity loss between pre- and post-irradiation scans of the film was converted to dose through the calibration fit equation. Figures 11 and 12 show line profiles through the axial and coronal slices, respectively. Maximum error calculated was ~3% between film and PRESAGE dose measurement – except for slight optical-CT dose under-estimation along the 3mm-narrow field. Further investigation is required to reconcile this dose

difference, which may be caused due to a stray light artifact that has been shown in previous work to effect regions of steep dose gradients with small fields[33].

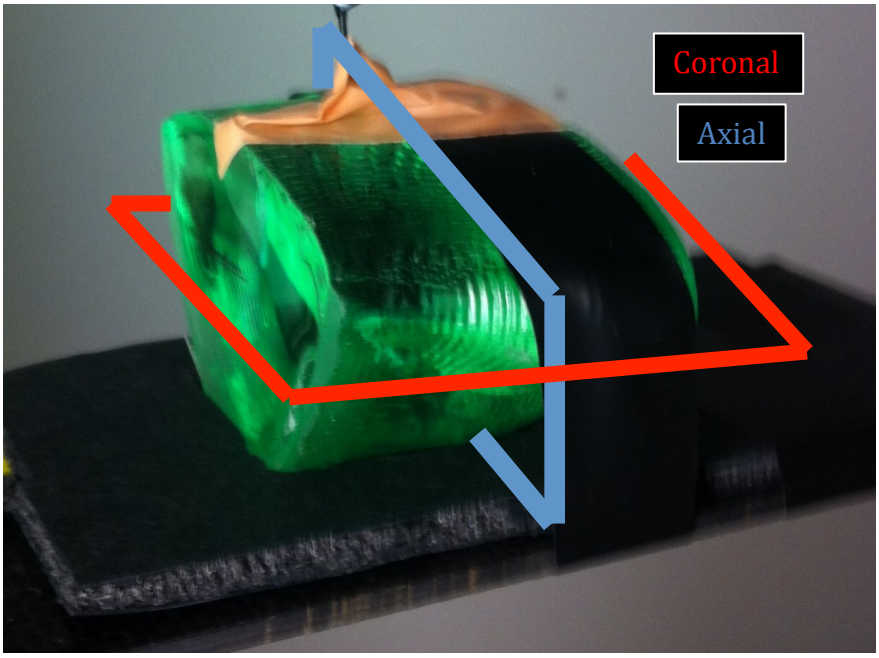

Figure 10 - Schematic showing placement of radiochromic film for independent measurement of dose distributions.

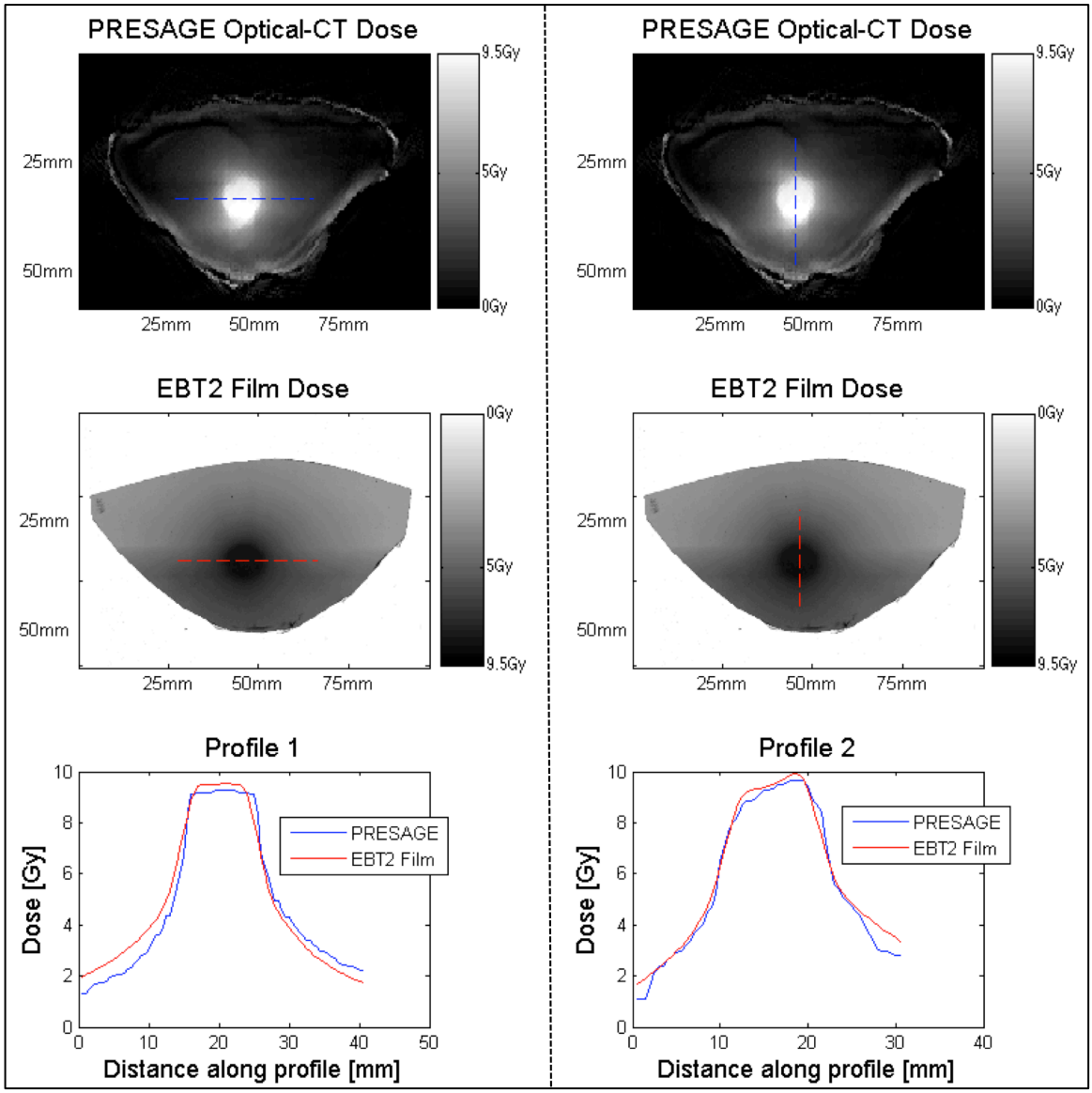

Figure 11 - Axial dose distributions measured with optical-CT (top row) and EBT2 film (middle row), with comparative line profiles (bottom row).

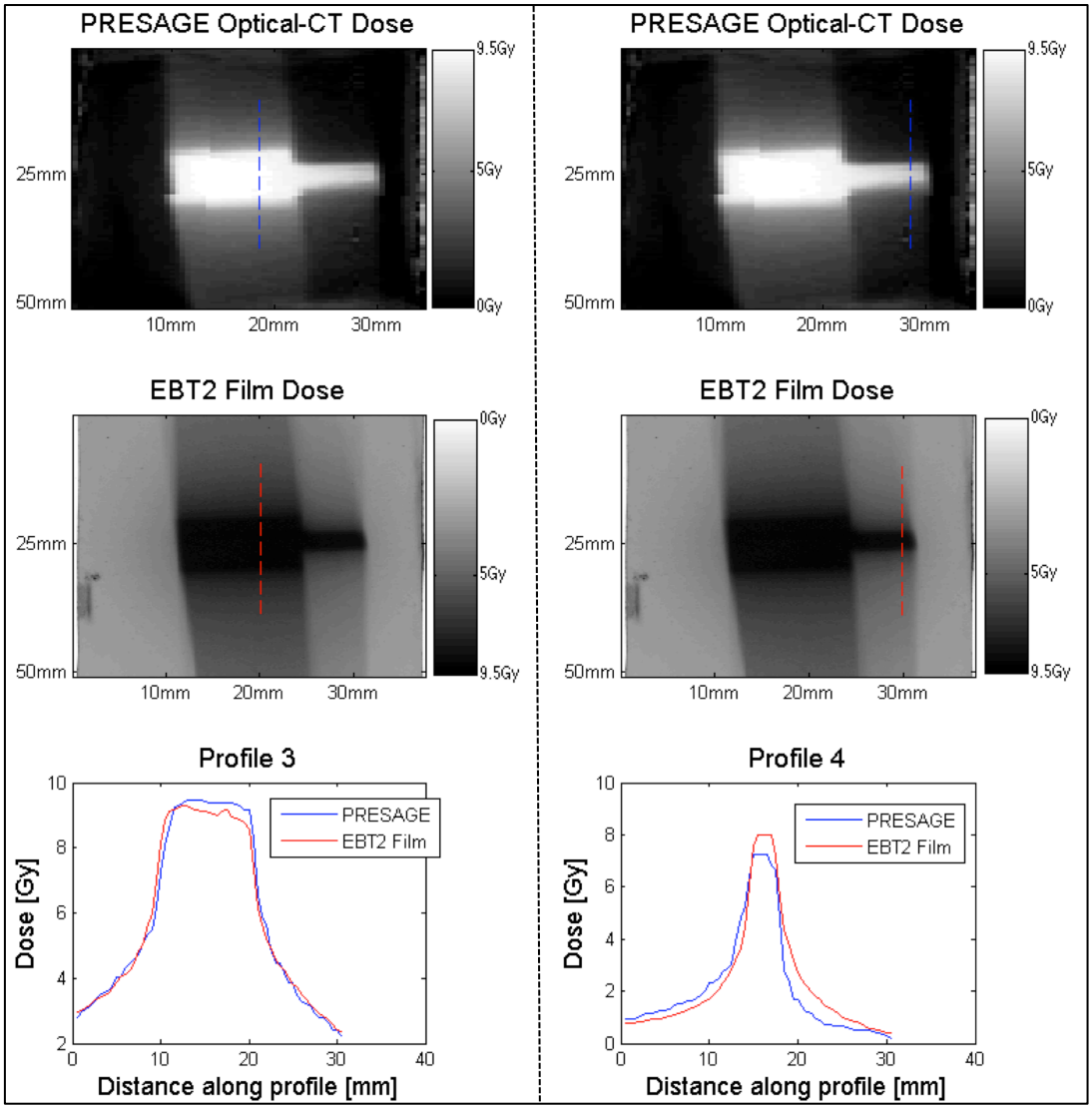

Figure 12 - Coronal dose distributions measured with optical-CT (top row) and EBT2 film (middle row), with comparative line profiles (bottom row). Profile 4 shows a dose underestimate with optical-CT. This may be due to partial volume effects in reproducing dose in the 3mm-wide field with 0.5mm voxels.

One benefit of rodent-morphic dosimeters is the ability to overlay dose distributions directly onto original rodent CT data. Figure 13 shows micro-SBRT dose distributions in transverse and coronal planes. Distributions as presented are assumed in homogeneous tissue. Future work is required for modification of dose from homogenous to heterogeneous rodent composition, including an investigation of optical-CT readout in PRESAGE dosimeters with heterogeneous inserts (such as spinal imaging insert presented here).

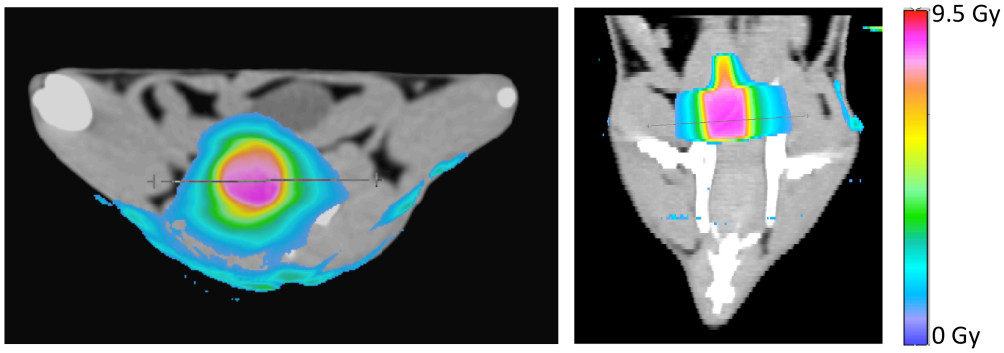

Figure 13 - PRESAGE dose distributions overlaid on original rat CT from which the 3D printing was made, in axial (left) and coronal (right) planes.

3.3.3 Mouse partial tumor irradiation pilot study

Recent research in tumor radiobiology has uncovered some progressive theories regarding the formation of metastatic cancers post-irradiation. Theoretically, the highly

use of conformal radiation beams pre-planned on high resolution patient CT data should minimize the risk of "missing" cancerous cells within the targeted region. The failure to irradiate a tumor volume in its entirety, known as a "marginal-miss", may have consequences other than just the survival of some cancer cells[34, 35].

The pre-clinical small animal setting is ideal for testing new ideas in tumor biology. Bold claims in the efficacy or consequences resulting from unique radiation treatments in small animals necessitate high resolution and accurate confirmation of dose distributions given by the small-animal irradiator.

In collaboration with a radiation biology group at Duke University, a homogenous rodent-morphic mouse dosimeter was produced directly from mouse CT data in the same fashion as described in Section 3.2. As of the time of this writing, several pilot studies have been performed to evaluate the feasibility of imaging optical-CT readouts and dose distributions in high-resolution (0.3mm isotropic) with a further scaled down analogue of the DLOS system, the DmicrOS.

3.3.3.1 Rodent-morphic mouse dosimeter

Figure 14 shows the 3D mesh file used for creation of the PRESAGE rodent-morphic dosimeter, as well as an optical-CT projection image of the resulting dosimeter. For this pilot study, a tumor volume was segmented to enable isocentric placement at one side of the tumor. The mouse phantom was placed in the prone position on the

carbon-fiber treatment stage of the X-Rad225Cx, with a lead block placed in the field to shield approximately half of the tumor volume. The mouse was then treated with simple anterior-posterior field. Currently being investigated is the dose drop-off at the interface between the irradiated and blocked tumor volume [Figure 15]. Future work will involve an investigation of a partial tumor arc treatment, as well as feasibility of accurate dose volume histogram (DVH) calculations from overlaying 3D dose distributions onto original mouse CT data.

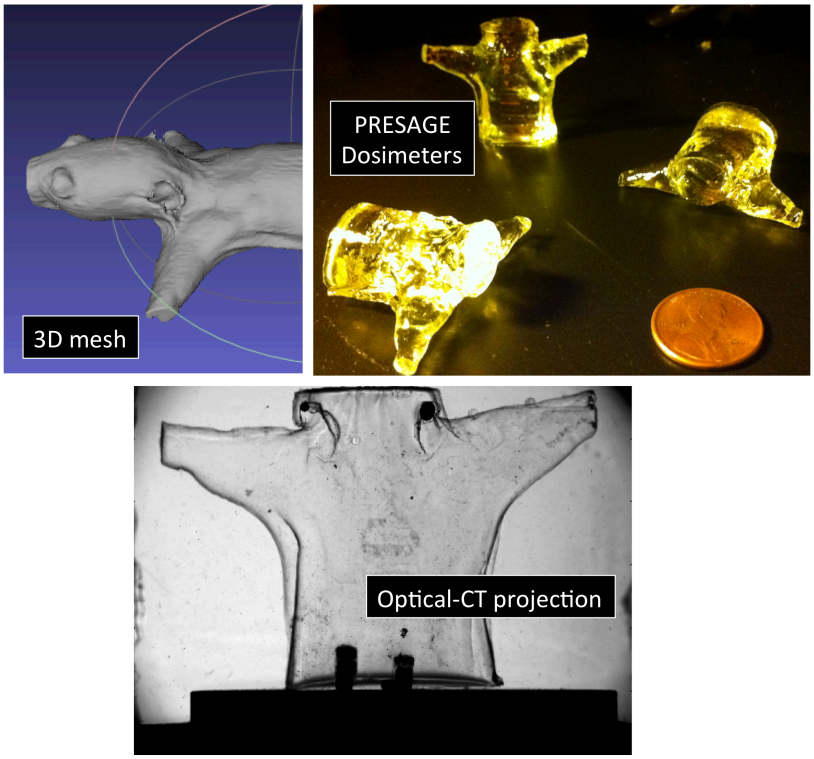

Figure 14 - 3D mesh file (top left) created from mouse CT data and used for PRESAGE mouse dosimeters (top right, American penny for scale). The bottom image shows an optical-CT projection taken with the DmicrOS system.

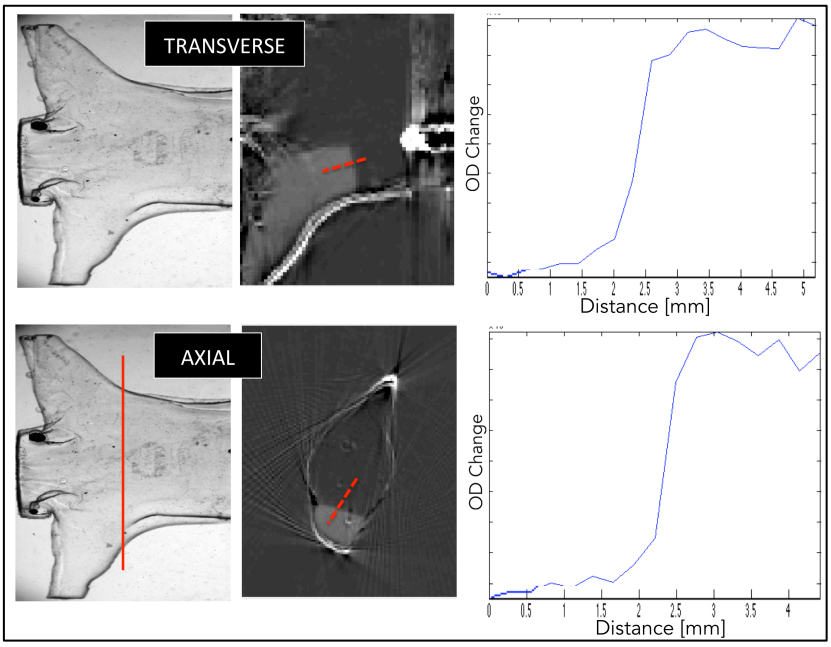

Figure 15 - Preliminary partial tumor-irradiation data showing sharp dose drop-off at full field/ blocked field interface.

3.4 Rodent-morphic dosimetry discussion

For the first time, accurate dose-distribution readout is available in high-resolution rodent-morphic phantoms for small animal micro-irradiators. Variable density PRESAGE provided adequate contrast to be a viable method of CBCT targeting and isocenter placement on the X-Rad225Cx irradiator, while optical-CT readout provides an accurate dose measurement when compared to direct exposure measurement. While this study focused on rat spine/outer body and mouse body

contours, any volume of interest may be segmented, converted to 3D-printible file, and made into a mold for PRESAGE anatomically accurate phantoms. This method of dose measurement allows for high-resolution of complex treatment paradigms being used in the pre-clinical setting, and enhances the robustness of tumor biology and radio-response studies in the small animal regime.

For future work, heterogeneous rodent-morphic dosimeters with one or more anatomical inserts will be investigated. Dose calculations with beams in the kV range are more sensitive to heterogeneous tissues, so an anatomically correct rodent-morphic dosimeter consisting of PRESAGE inserts of varying effective-Z would be more ideal for high-resolution dose readout given by small animal irradiators. PRESAGE-def is a dosimeter formulation able to be deformed with 3 degrees of freedom and relaxed back into the initial size and shape. Complex deformation of human organs (i.e. liver, lungs) may also be simulated through 3D printing of human anatomy and production of anatomically accurate anthropomorphic dosimeters. This may be accomplished using the same series of production steps presented here.

4. Feasibility of 'Dry' Scanning

One of the distinct challenges in optical-CT is the method for directing incident light through a sample and into a detector or CCD array in a straight path with minimal deviation due to refraction at the air/dosimeter interfaces. Telecentric lenses may be used to achieve parallel-beam geometry for the incident light, while immersing the dosimeter in a fluid of similar refractive index minimizes refraction.

For this work, two questions were addressed: (1) Can the bulky, expensive, telecentric lenses be replaced by a more manageable Fresnel lens system? And (2) can the cumbersome refractive index-matching fluid be minimized[36, 37]? This work introduces the Duke Fresnel dry Optical-CT System (DFOS), an analogue to the Duke Large-field Optical-CT System (DLOS), but with modifications to address these optical-CT challenges.

4.1 DFOS

The DFOS system replaces the convex telecentric lenses used in the DLOS system with a Fresnel lens system (Light Works, Toledo, OH), resulting in cost savings of around 99% (~$4000 to ~$40), and a lens weight reduction from ~7kg to 500g [Figure 16]. Fresnel lenses have inherent non-uniformity due to the Fresnel grooves, and a Moiré effect is noticeable when imaging with a pair of lenses in a telecentric setup.

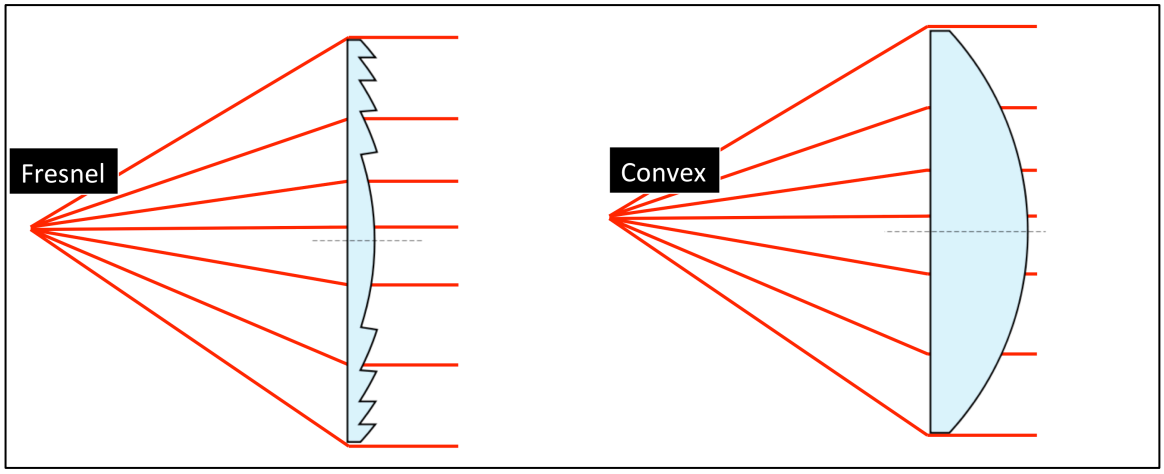

Figure 16 - Comparison of parallel-beam collimation from Fresnel and Convex lenses. Equivalent power Fresnel lenses may be 100X less expensive and close to 15X lighter than convex collimating lenses.

Non-uniformities from the Fresnel lenses can be reduced by: (1) ensuring proper focus of the system directly between the pair of lenses, and (2) decreasing the aperture (focal ratio) of the lens at the camera side (increasing the f-number, illustrated in Figure 17), while increasing the LED output aperture. The decreased aperture at the camera side allows for a larger field-of view, and reduces the sensitivity to slight-refractive variations form the Fresnel lens. Any remaining imperfections or non-uniformities should be theoretically corrected for by taking projection images both before and after dosimeter irradiation.

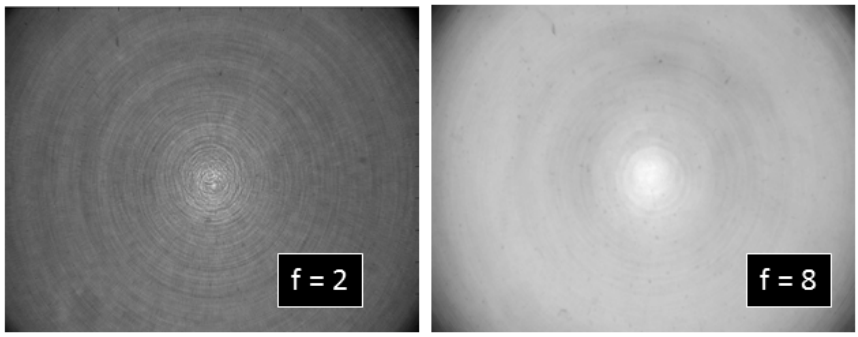

Figure 17 - Non-uniformities caused by Fresnel grooves (left) may be reduced by increasing the f-stop (right) at the imaging lens. Remaining non-uniformities are corrected by acquiring pre- and post-irradiation images.

Another modification to the DLOS system present in the DFOS is the minimal fluid bath. Refractive index matching fluid is used in optical-CT to allow incident light to pass through the dosimeter in a parallel path without refraction at the interface between two media. For the DFOS system, the glass aquarium was replaced with a 17x17x17 cm^3 polyurethane cube with a cylindrical bore of diameter 11.5cm and height 10cm, allowing for placement of an 11cm diameter x 10cm dosimeter. The 2.5mm air gap surrounding the dosimeter requires ~90 cm^3 of fluid of match the refractive index between the polyurethane tank (RI = 1.5) to PRESAGE dosimeters (RI = 1.47-1.51), compared to ~13500 cm^3 of fluid for the DLOS system.

In the absence of a dosimeter, the "dry" polyurethane tank essentially becomes an air-gap, refracting all incident light out of the CCD field-of-view. Theoretically, an incident light image or "flood" field may be acquired by filling the tank with fluid matched to the polyurethane tank. This would not only require *more* fluid handling, but

an RI mismatch between the tank (and fluid used for flood) and dosimeter would cause a loss of signal at the dosimeter edges, manifesting as dark bands [Figure 18]. For all DFOS image acquisitions, the flood field image was purposefully omitted. This assumes that the LED output, and therefore incident light, remains constant between pre- and post-irradiation scans.

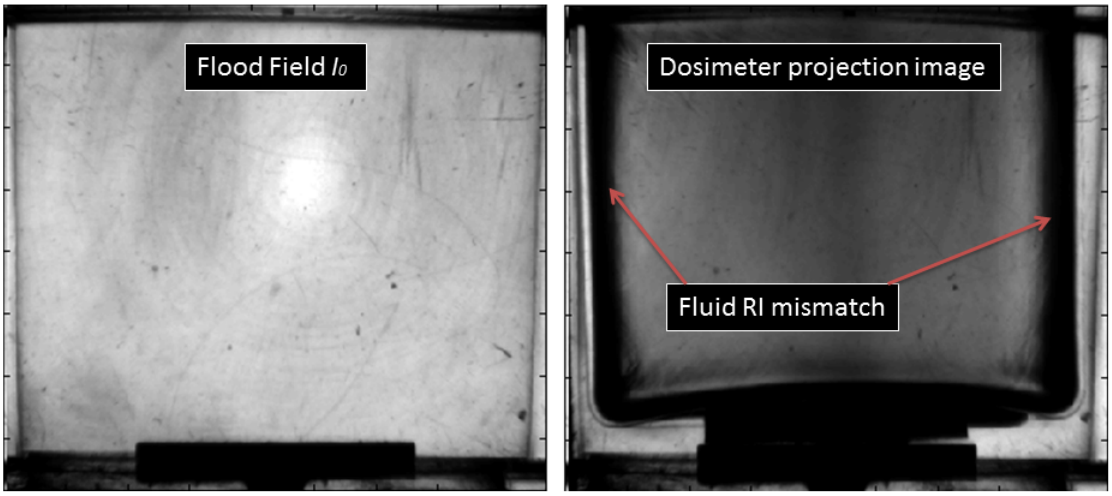

Figure 18 - Flood field acquired by filling the DFOS polyurethane tank with RI-matching fluid (left). Matching the fluid to the tank achieves good uniformity all the way to the edges, but immersing a dosimeter of different refractive index into the fluid causes mismatching artifacts at the edge (right). This phenomena, combined with the desire to minimize fluid handling, drove the decision to omit the flood field altogether.

To investigate the consequence of omitting the flood field, high dynamic range DLOS data was reconstructed both with and without flood fields and compared. Figure

19 shows dose line profiles through 3 Gy, 6 Gy, and 9.5 Gy dose regions both with and without flood fields, and corresponding dose error assuming PRESAGE dosimeter with sensitivity 0.05 OD change/cm-Gy (a typical value seen in PRESAGE formulations). Maximum dose error for this representative case was 4.6 cGy, occurring in the 6 Gy dose region. This corresponds to a 0.77% absolute dose difference. Further investigation into the LED consistency and the validity of flood field omission is required.

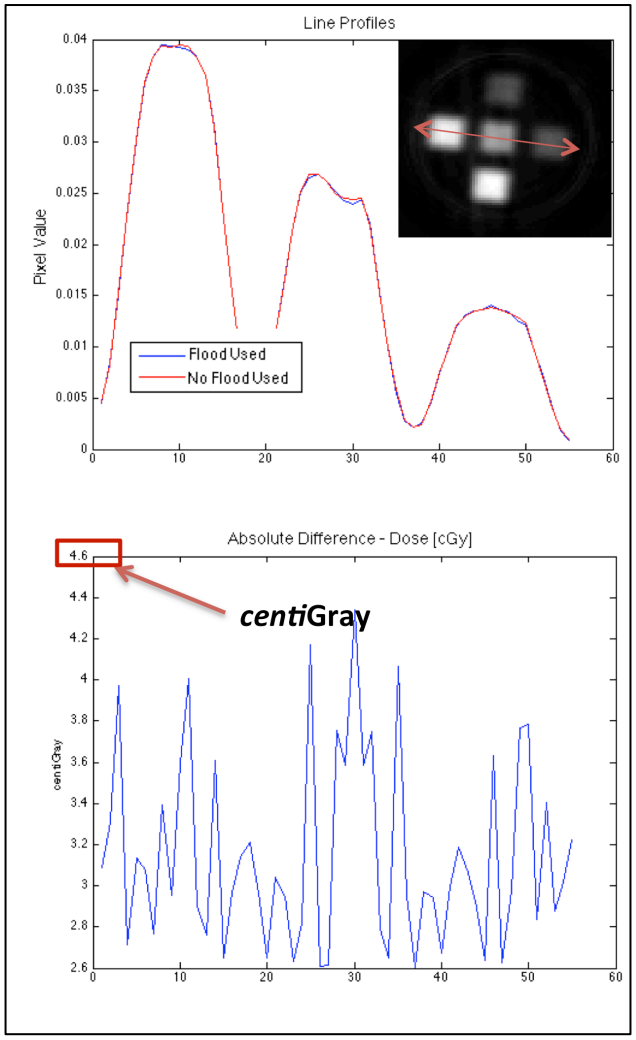

Figure 19 - Comparison of line profile through a slice reconstructed with and without a flood field projection. Maximum computed dose error in this case is only 4.2 cGy.

4.2 Treatment plans

To evaluate the DFOS system, 3 treatments were given to PRESAGE radiochromic dosimeters. For all treatments, CT scans were taken of the dosimeter and imported to the Eclipse (Varian Medical Systems, Palo Alto, CA) treatment planning

software (TPS) for dose prediction for each treatment. Dose was delivered by 6MV beams at a dose rate of 600 MU/min for all irradiations. Comparisons were made varying dosimeter formulations, treatment plans, and optical-CT systems, by computing the gamma passing rate at a threshold of 3%/3mm with respect to TPS prediction for all optical-CT reconstructions. Table 2 below shows a summary of all irradiation plans, scanner comparisons, and dosimeter formulations. For this preliminary study, relative dose was converted to absolute dose by making a point measurement in the Eclipse predicted dose distribution and scaling the optical-CT reconstructed OD-change accordingly. This step was justified as PRESAGE has been shown to exhibit a strong linear optical density change with absorbed dose.

Table 2 – Summary of all scanner comparison parameters, including: treatment description, dosimeter formulation description, systems being compared, and delay between treatment and post-irradiation scan.

Irradiation		Optical-CT Comparisons		Dosimeter Formulation			
Name	Fields	Systems	Readout post-irradiation	Name	Leuco-Dye	Solvent	[Initiator]
Parallel-opposed I	4-field 4cm x 10cm	Eclipse TPS DFOS	0 hrs	DX	LMG (2.0%)	cyclo-hexanone (7.0%)	0.75%
Parallel-opposed II	4-field 4cm x 12cm	Eclipse TPS DFOS DMOS DLOS	20 hrs	DEA -1	O-MeO-LMG-DEA (1.5%)	butyl acetate (5.0%)	0.4%
Brain IMRT	5-field IMRT	Eclipse TPS DFOS DLOS	3 hrs	DEA -1	O-MeO-LMG-DEA (1.5%)	butyl acetate (5.0%)	0.4%

4.2.1 Rectangular orthogonal parallel-opposed treatment I

The first treatment consisted of two orthogonal sets of parallel-opposed 4cm x 10cm beams, delivered to a cylindrical 11cm diameter x 10cm PRESAGE dosimeter. Dose was configured in order to have 3 distinct dose regions by delivering 200 monitor units each for the right/left lateral and left/right lateral beams (low dose) and 300 monitor units each for the anterior/posterior and posterior/anterior beams (medium dose), leaving a high dose cube in the center of the distribution [Figure 20]. Projection images were taken over 360-degrees at 1-degree increments with the DFOS scanner both before and after irradiation and reconstructed at 2mm resolution with a custom MATLAB GUI.

4.2.2 Rectangular orthogonal parallel-opposed treatment II

The second irradiation was similar to irradiation 1, with the key difference being a comparison between 3 available scanners – the DMOS, DLOS, and DFOS – relative to Eclipse TPS. An 11cm diameter x 10cm dosimeter was irradiated with two sets of parallel opposed beams, with dose again being separated into three distinct regions [Figure 20]. For all 3 optical-CT systems, 360 projections were acquired at 1-degree increments and reconstructed with 2mm isotropic voxels.

4.2.3 Brain IMRT treatment

The final irradiation was performed on a third cylindrical 11cm diameter x 10cm PRESAGE dosimeter. Treatment consisted of a 5-field brain IMRT plan to be delivered to the cylindrical dosimeter through a plastic tissue-equivalent head phantom [Figure 20]. Projection images were taken again at 360 1-degree increments and reconstructed at 2mm resolution with both the DLOS and DFOS systems, to enable comparison of DFOS performance with both Eclipse prediction and the gold-standard DLOS system. Comparison of both reconstructions with Eclipse prediction were again preformed by computing the 3%/3mm gamma index.

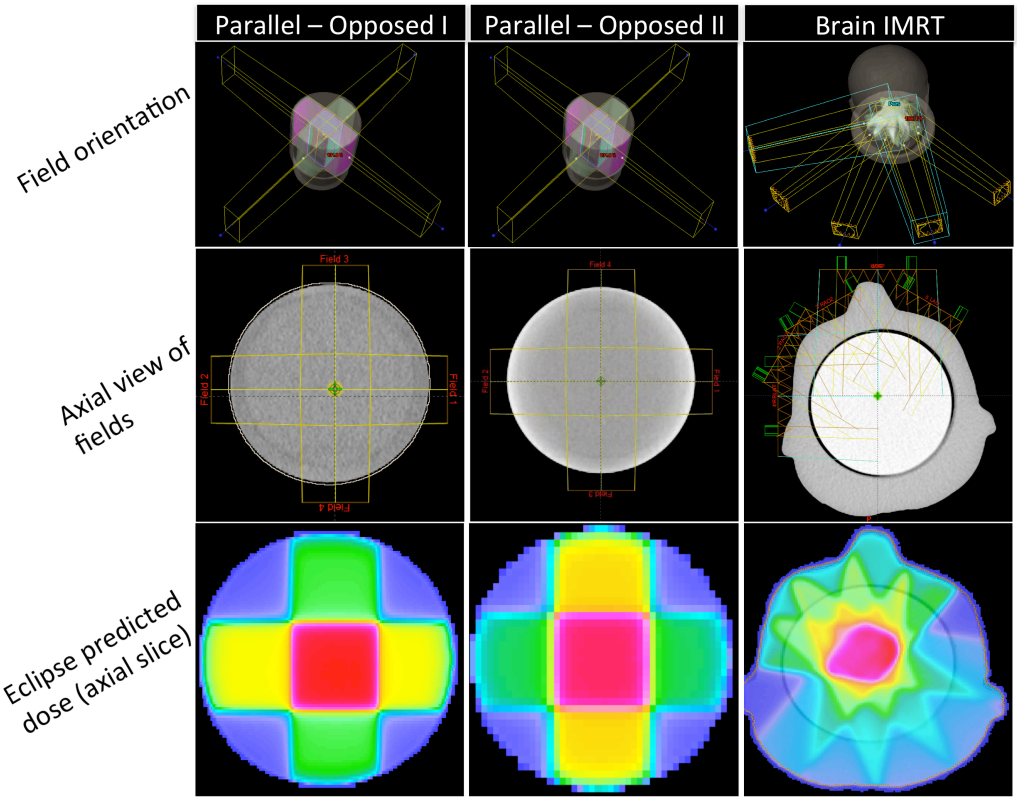

Figure 20 - Rectangular parallel-opposed I (left), II (center) and five-field brain IMRT (right) treatment plans from Eclipse TPS.

4.3 Results of 'Dry' Scan Comparison

Initial comparison of DFOS dose distributions showed promising results. DFOS reconstruction for parallel-opposed treatment plan I had a gamma index pass rates of 89.3% with a 3%/3mm criteria compared to Eclipse TPS prediction, showing promise but substantially less accurate than desired. For the brain IMRT plan, the DFOS dose had a gamma pass rate of 87.5% - again promising but not optimal when compared to the

DLOS gamma pass rate of 99.0% for the same treatment. For the parallel-opposed treatment II, the DFOS, DLOS, and DMOS were all compared with Eclipse prediction. A slight rounding of all steep dose gradients was observed with all three systems – which may be due to dosimeter formulation changes or diffusion of signal between irradiation and post-iradiation scanning, which was performed 20 hours later. However, the gamma pass rates for the DFOS, DLOS, and DMOS were 92.2%, 95.6%, and 96.8%, respectively, compared to Eclipse prediction. It should be noted that DLOS and DMOS distribution matched almost perfectly (99.0% when compared to each other), showing both systems to be performing optimally at this time. Table 3 below summarizes all gamma pass rates for all treatments compared to Eclipse TPS prediction.

Table 3 – Summary of gamma 3%/3mm pass rates for all irradiations

Irradiation		Dosimeter	Gamma pass rate
Name	**Fields**	**Formulation Name**	**3%/3mm compared to Eclipse TPS**
Parallel-opposed I	4- field 4cm x 10cm	DX	DFOS = 89.3%
Parallel-opposed II	4-field 4cm x 12cm	DEA-1	DFOS = 92.2% DMOS = 96.8% DLOS = 95.6%
Brain IMRT	5-field IMRT	DEA-1	DFOS = 89.3% DLOS = 99.0%

Figure 21 shows orthogonal slices of predicted and measured dose for the parallel-opposed plan I, along with gamma views. Figures 22-25 show orthogonal views for the parallel-opposed II [Figure 22] and brain IMRT [Figure 24] plans for predicted and optical-CT measured dose show orthogonal views of predicted and measured dose, while Figures 23 and 25 show gamma map slices for the parallel-opposed II treatment and brain IMRT treatment, respectively.

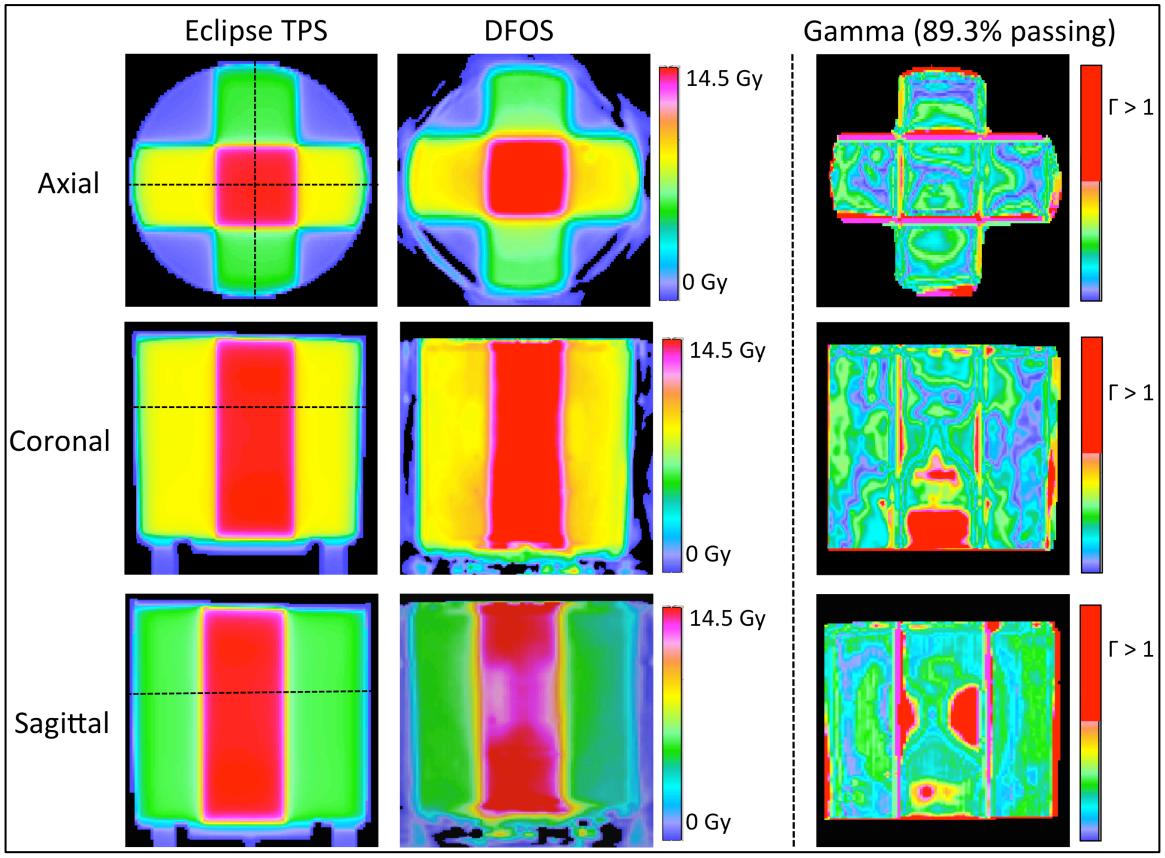

Figure 21 - Eclipse predicted dose (left), DFOS reconstructed dose (middle) and 3%/3mm gamma maps (right) for three orthogonal planes in parallel-opposed treatment plan I.

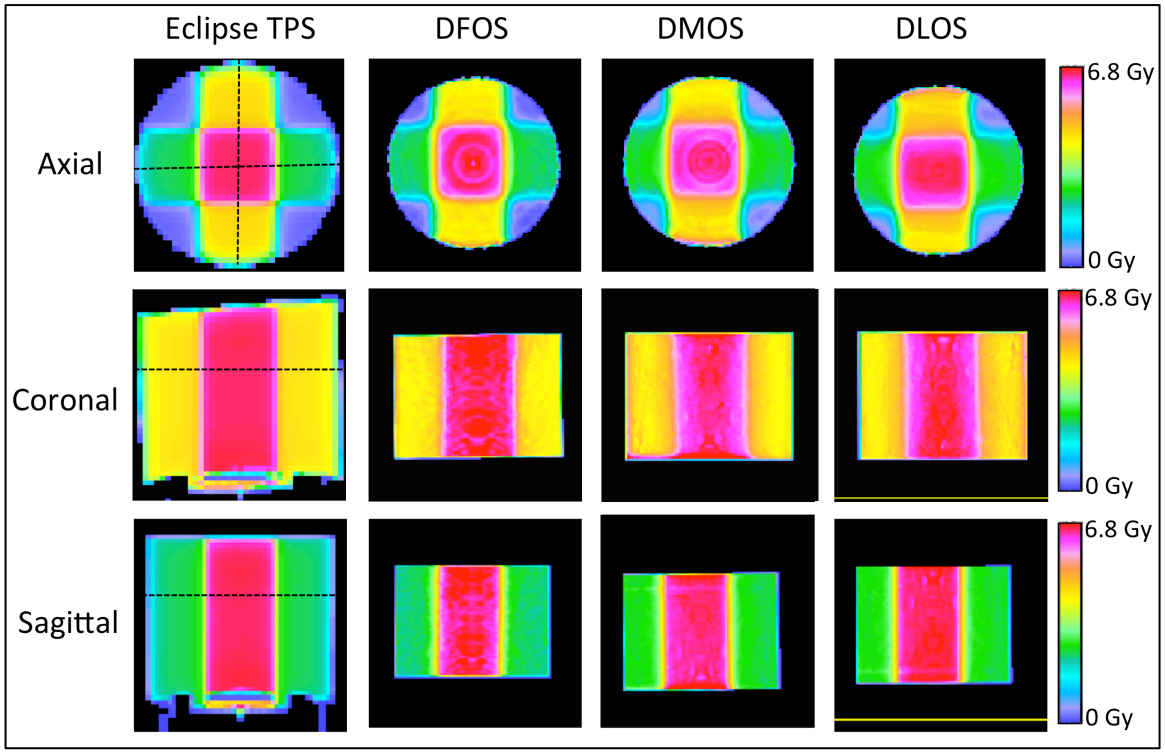

Figure 22 - Eclipse predicted dose (left), DFOS reconstructed dose (second column), DMOS reconstructed dose (third column) and DLOS reconstructed dose (right) for three orthogonal planes in parallel-opposed treatment plan II.

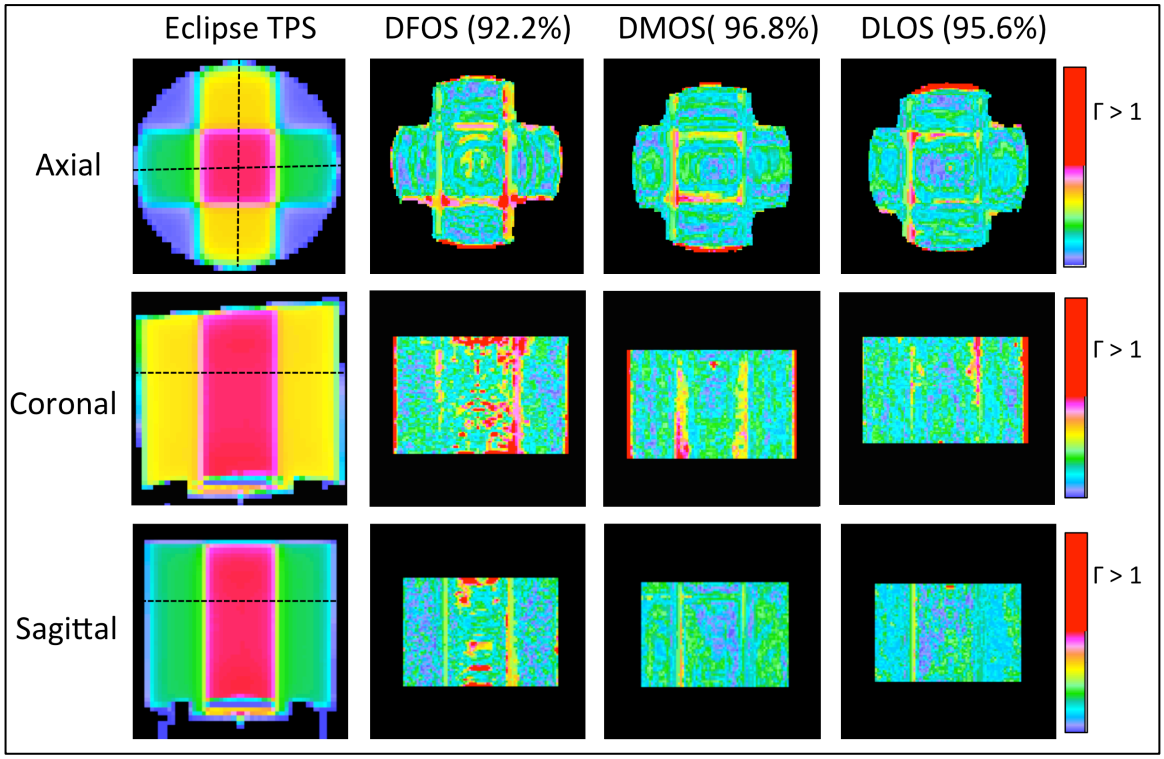

Figure 23 - Three orthogonal views of 3%/3mm gamma maps for DFOS (column 2), DMOS (column 3), and DLOS (right) systems, with passing rates. Eclipse dose views (left) for reference.

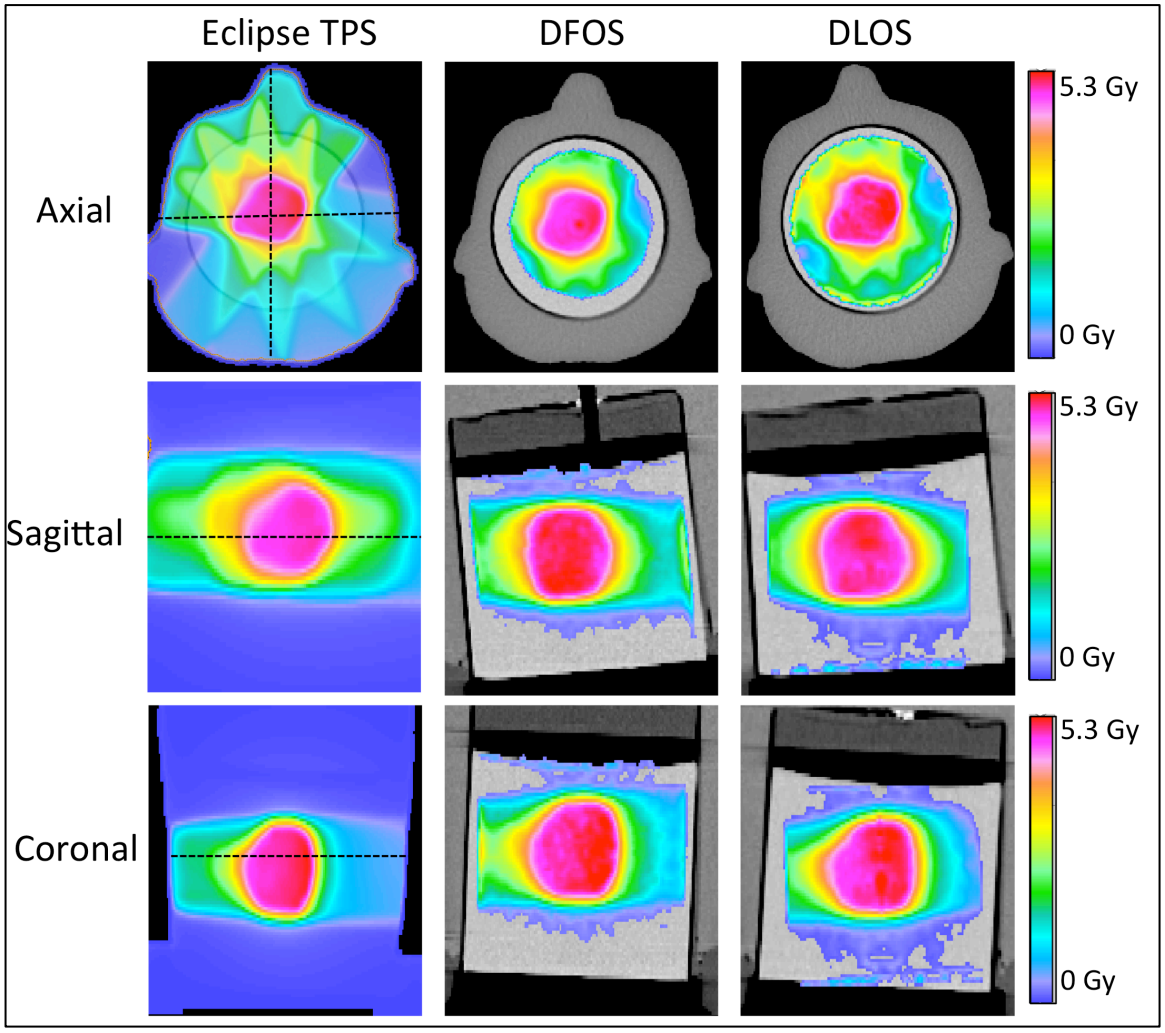

Figure 24 - Eclipse predicted dose (left), DFOS reconstructed dose (middle) and DLOS dose (right) for three orthogonal views in brain IMRT plan.

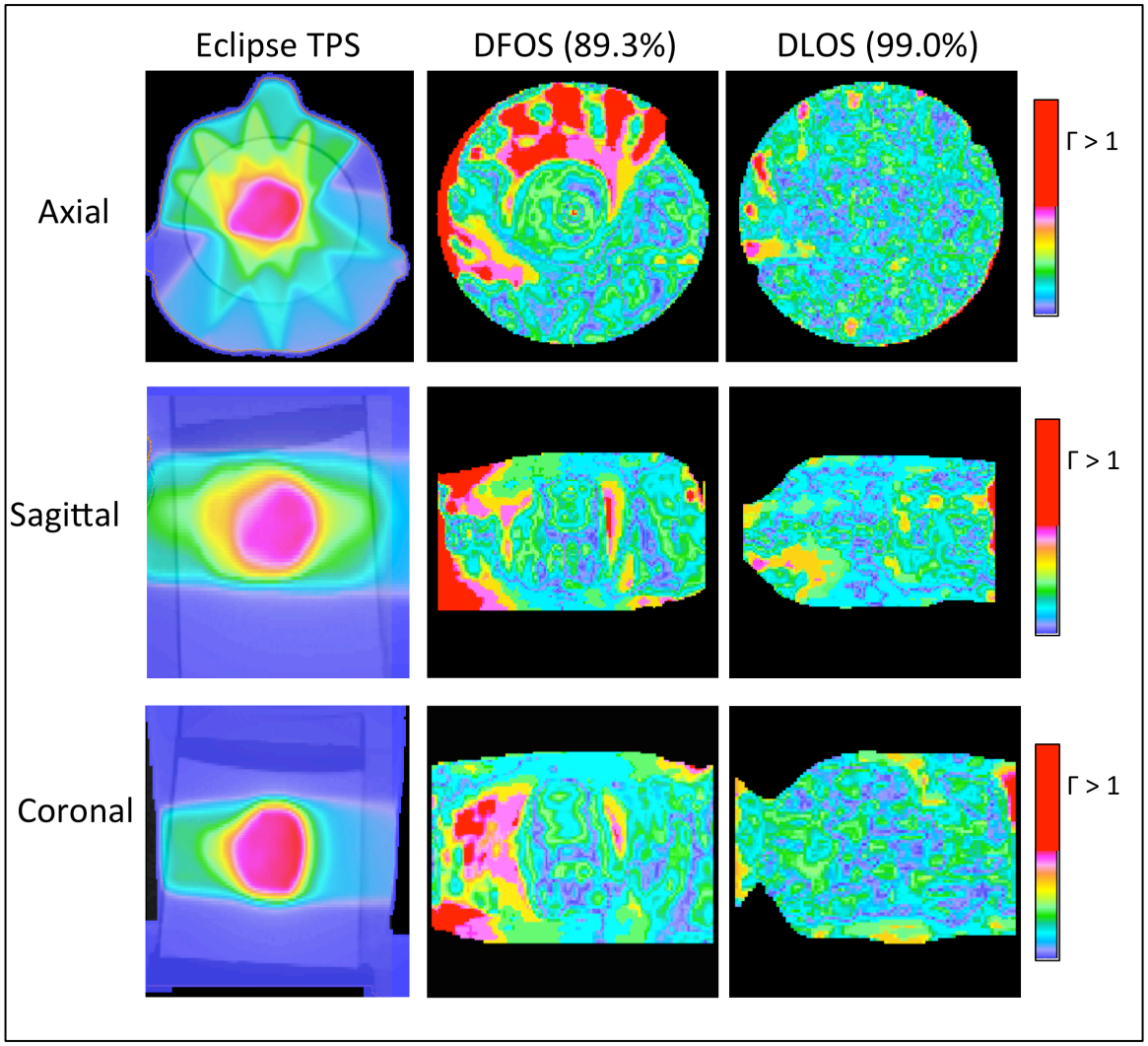

Figure 25 - Three orthogonal views of 3%/3mm gamma maps for DFOS (column 2) and DLOS (right) systems, with passing rates. Eclipse dose views (left) for reference.

The following figures [Figures 26-34] show line profiles through various orthogonal planes for each of the 3 treatment plans. Some notable takeaways – the DLOS system performed optimally for reproducing brain IMRT dose distributions,

while the DMOS matched the DLOS in the second parallel-opposed treatment. DFOS line profiles show a substantial increase in noise when compared to DLOS and DMOS reconstructions. Although concurrent work showed the optimal dose-readout time for the DEA PRESAGE formulation to be 3-24 hours post-irradiation, there is a significant rounding of sharp dose gradients shown with the all three systems in the second parallel-opposed treatment, which was readout ~20 hours post-irradiation. This is in comparison to a near perfect representation with the DLOS IMRT reconstruction, which features sharp dose gradients as well, but with readout performed 3 hours post-irradiation. Further investigation is needed to determine the reason for these inconsistencies.

4.3.1 Line Profiles – Parallel-opposed treatment I

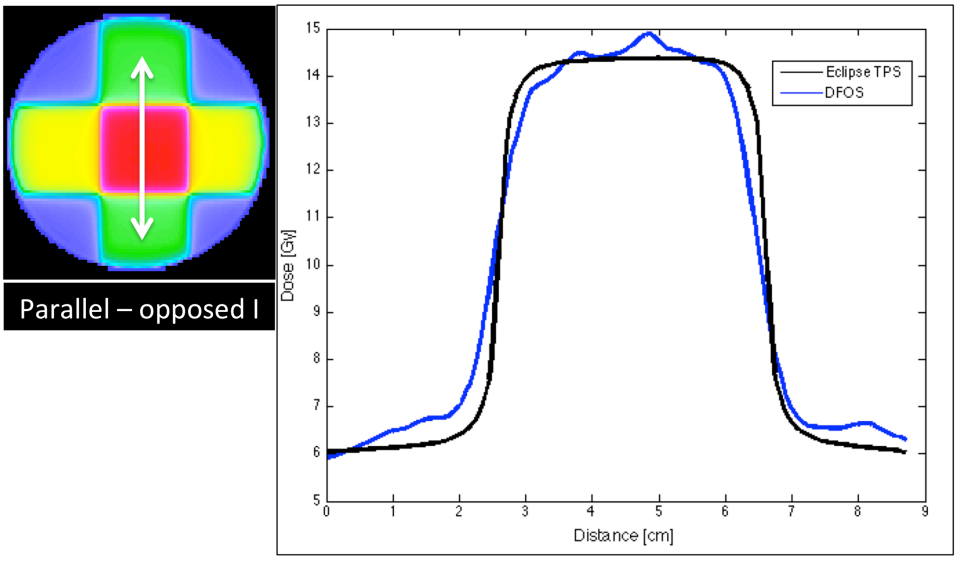

Figure 26 - Line profiles for parallel-opposed treatment I comparing Eclipse prediction (black), and DFOS dose (blue).

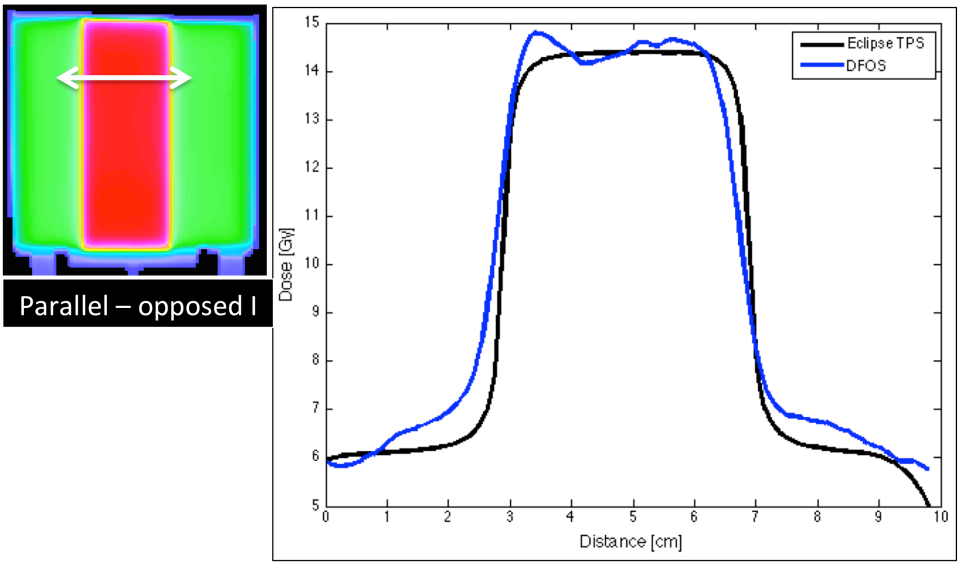

Figure 27 - Line profiles for parallel-opposed treatment I comparing Eclipse prediction (black), and DFOS dose (blue).

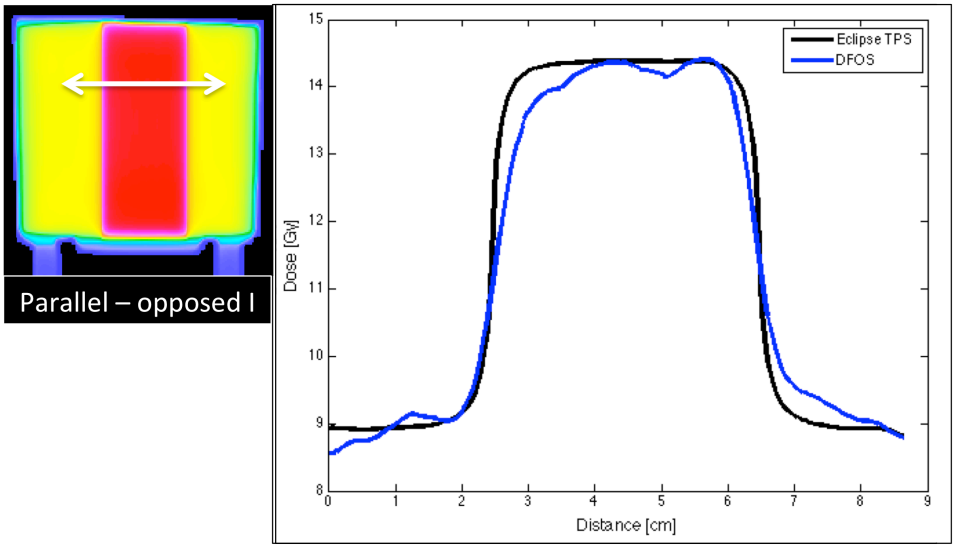

Figure 28 - Line profiles for parallel-opposed treatment I comparing Eclipse prediction (black), and DFOS dose (blue).

4.3.2 Line Profiles – Parallel-opposed treatment II

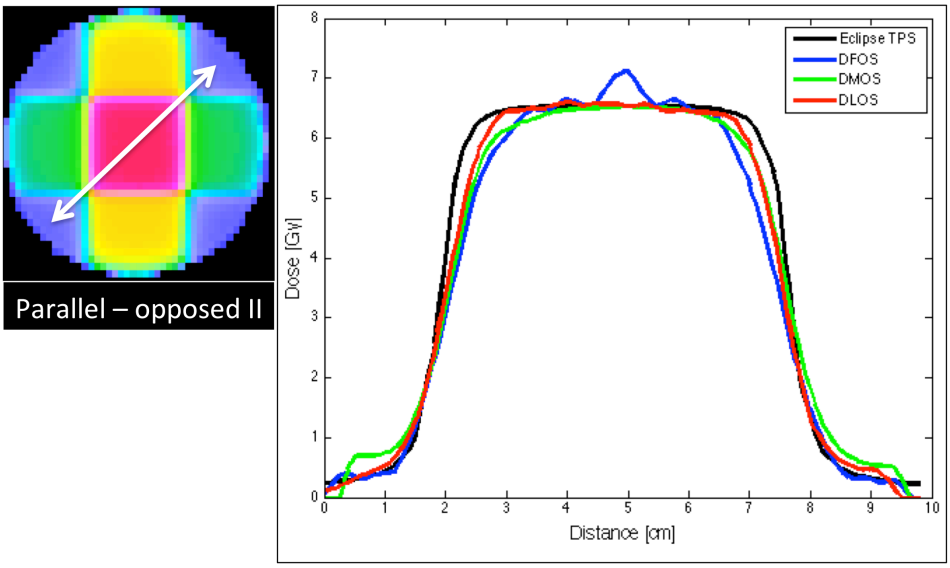

Figure 29 - Line profiles for parallel-opposed treatment II comparing Eclipse prediction (black), DFOS (blue), DMOS (green), and DLOS (red) dose.

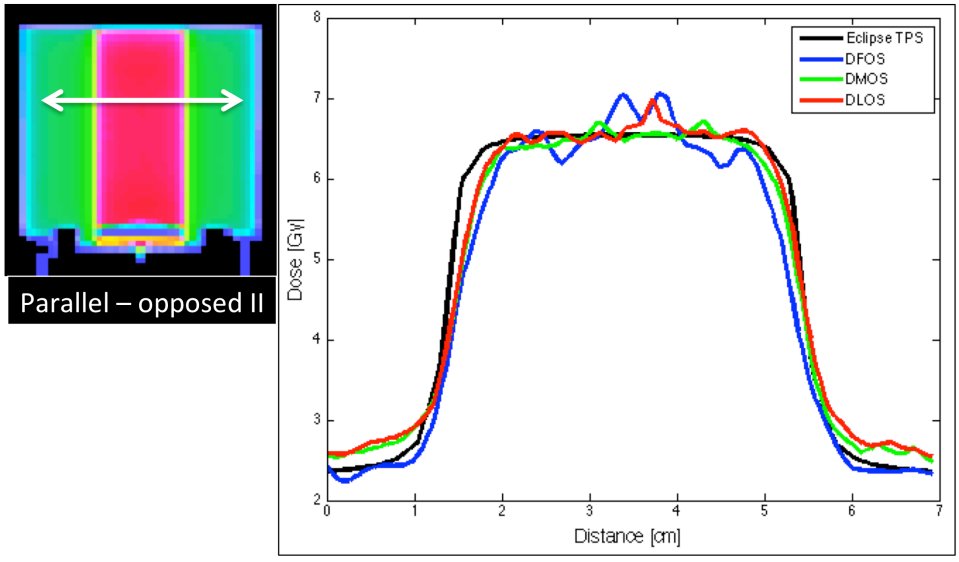

Figure 30 - Line profiles for parallel-opposed treatment II comparing Eclipse prediction (black), DFOS (blue), DMOS (green), and DLOS (red) dose.

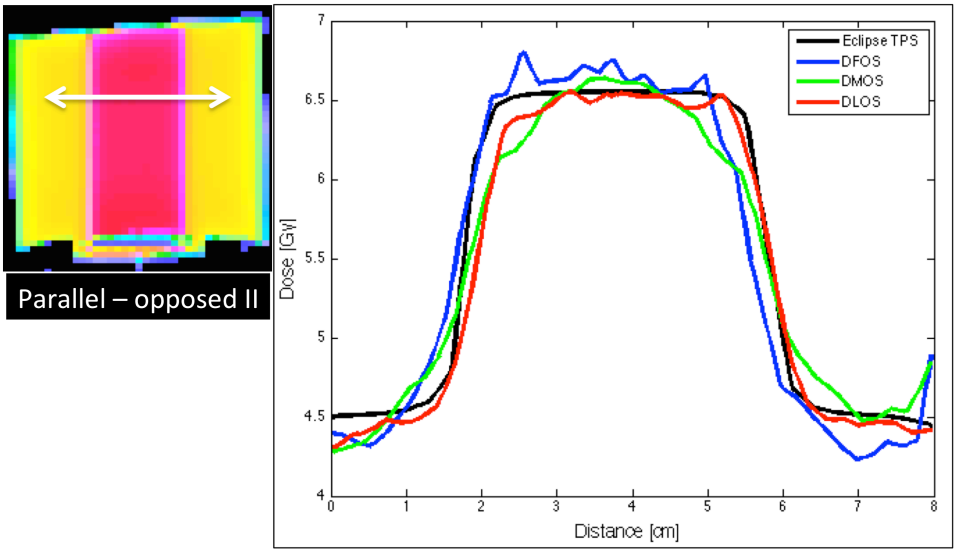

Figure 31 - Line profiles for parallel-opposed treatment II comparing Eclipse prediction (black), DFOS (blue), DMOS (green), and DLOS (red) dose.

4.3.3 Line Profiles – Brain IMRT treatment

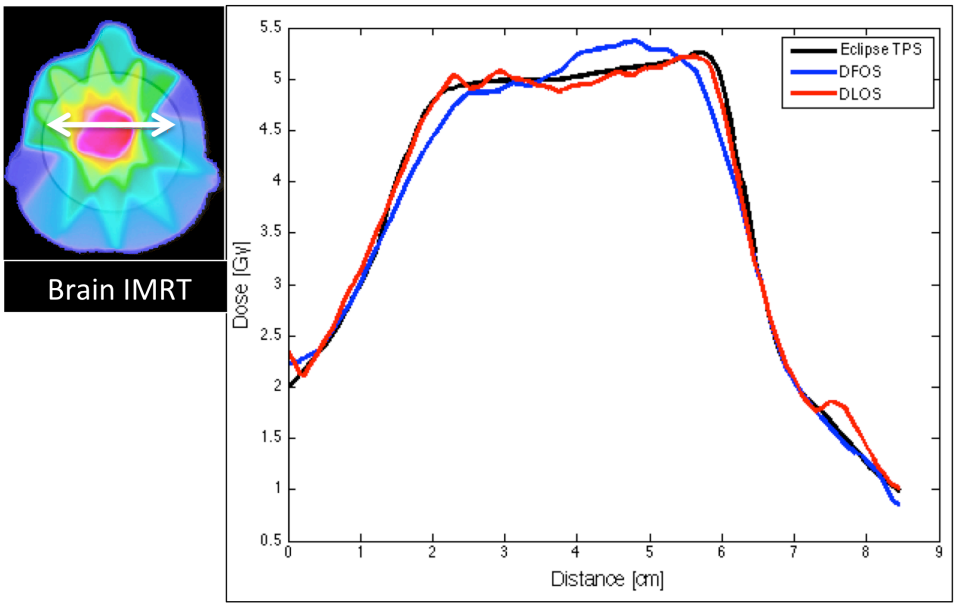

Figure 32 - Line profiles for brain IMRT treatment comparing Eclipse prediction (black), DFOS (blue), and DLOS (red) dose.

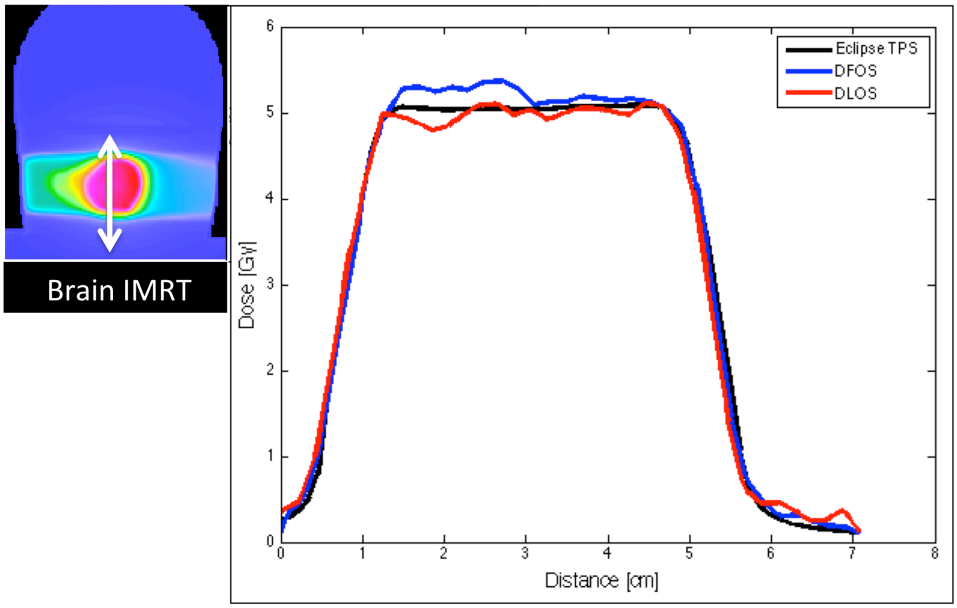

Figure 33 - Line profiles for brain IMRT treatment comparing Eclipse prediction (black), DFOS (blue), and DLOS (red) dose.

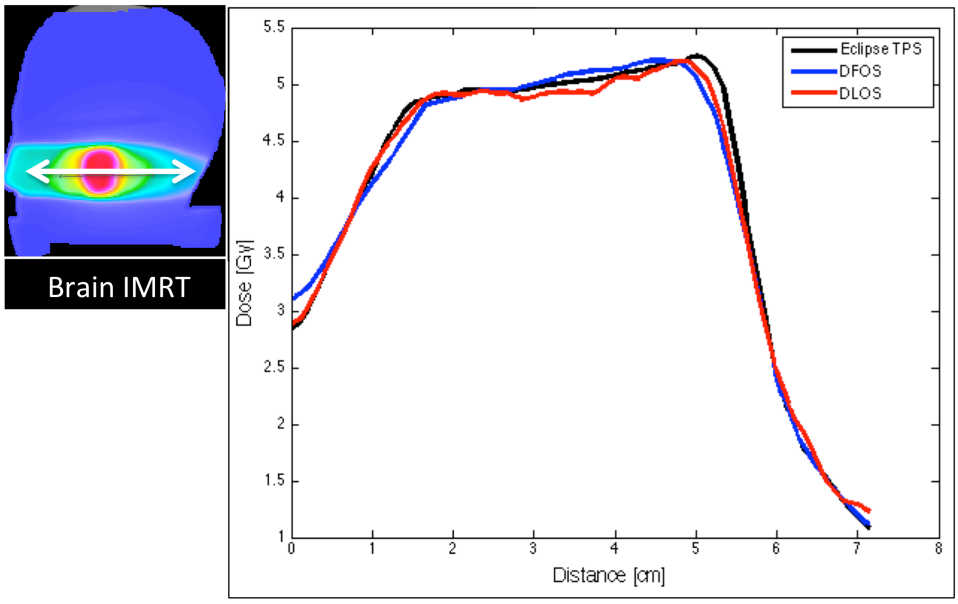

Figure 34 - Line profiles for brain IMRT treatment comparing Eclipse prediction (black), DFOS (blue), and DLOS (red) dose.

4.4 'Dry' Scan Discussion

Because of the two drastic changes incorporated into the DFOS system, several considerations must be made when comparing with the current gold standard DLOS system. The Fresnel lenses produce obvious non-uniformities in the incident light field, which can only be corrected for when alignment is reproduced exactly between the pre- and post-irradiation scans. Therefore, special attention needs to be paid to avoiding any changes in setup geometry. Minimizing the fluid necessary for "dry" scanning has obvious implications for the practicality of optical-CT, as well as decreasing the likelihood of imperfections in the fluid bath causing ring artifacts in the reconstructed image.

Overall, first attempts for imaging 3D dose distribution with an optical-CT system with minimal fluid and Fresnel lenses is promising. The largest source of error seems to be regions of high optical attenuation. Further investigation is required to improve 3%/3mm gamma pass rates from the 85-90% range. With a gamma pass rate of 99%, the DLOS gold standard system is performing optimally, with the DMOS system seeming to match DLOS performance.

5. Conclusion

As we learn more about the biological mechanisms behind both the spread of cancer and the tumor response to radiation therapy, the small animal pre-clinical setting will become an increasingly significant scientific realm. Small animal radio-response research gives new theoretical insights into radiation therapy. These small animal platforms give an opportunity to make the translation from small cell-line studies and simulations to human care in much the same way that clinical trials for drugs are carried out presently. As our understanding of tumor radio-response becomes more "high-resolution", a similarly high-resolution verification of doses given in the pre-clinical setting is essential.

In this work a powerful new pre-clinical tool for high-resolution 3D dosimetry in anatomically accurate rodent phantoms was presented and verified. Although only a mouse and rat were studied, this workflow allows any anatomy of interest to be scanned and printed into a 3D dosimetric phantom, with varying densities and compositions. Optical-CT with PRESAGE rodent-morphic dosimeters was shown to be accurate. Challenges related to cost and convenience involved in the acquiring of optical-CT images were also addressed, with the Duke Fresnel-based Optical-CT System (DFOS) showing much promise as a practical and viable system, although currently well behind the capability of the telecentric lens based DMOS and DLOS system.

References

[1] F. Verhaegen, "Small-animal irradiation: precision platforms emerge," (Medical Physics Web, medicalphysicsweb.org, 2011).

[2] F. Verhaegen, P. Granton, E. Tryggestad, "Small animal radiotherapy research platforms," Physics in Medicine and Biology **56**, R55-83 (2011).

[3] M. Matinfar, I. Iordachita, E. Ford, J. Wong, P. Kazanzides, "Precision radiotherapy for small animal research," Medical image computing and computer-assisted intervention **11**, 619-626 (2008).

[4] M. Rodriguez, R. Jeraj, "Design of a radiation facility for very small specimens used in radiobiology studies," Physics in Medicine and Biology **53**, 2953-2970 (2008).

[5] J. Wong, E. Armour, P. Kazanzides, I. Iordachita, E. Tryggestad, H. Deng, M. Matinfar, C. Kennedy, Z. Liu, T. Chan, O. Gray, F. Verhaegen, T. McNutt, E. Ford, T.L. DeWeese, "High-resolution, small animal radiation research platform with x-ray tomographic guidance capabilities," International Journal of Radiation Oncology, Biology, Physics **71**, 1591-1599 (2008).

[6] K.H. Song, R. Pidikiti, S. Stojadinovic, M. Speiser, S. Seliounine, D. Saha, T.D. Solberg, "An x-ray image guidance system for small animal stereotactic irradiation," Physics in Medicine and Biology **55**, 7345-7362 (2010).

[7] E. Tryggestad, M. Armour, I. Iordachita, F. Verhaegen, J.W. Wong, "A comprehensive system for dosimetric commissioning and Monte Carlo validation for the small animal radiation research platform," Physics in Medicine and Biology **54**, 5341-5357 (2009).

[8] P.V. Granton, F. Verhaegen, "On the use of an analytic source model for dose calculations in precision image-guided small animal radiotherapy," Physics in Medicine and Biology **58**, 3377-3395 (2013).

[9] S.J. van Hoof, P.V. Granton, F. Verhaegen, "Development and validation of a treatment planning system for small animal radiotherapy: SmART-Plan," Radiotherapy and Oncology : Journal of the European Society for Therapeutic Radiology and Oncology **109**, 361-366 (2013).

[10] F. Verhaegen, S. van Hoof, P.V. Granton, D. Trani, "A review of treatment planning for precision image-guided photon beam pre-clinical animal radiation studies," Zeitschrift fur Medizinische Physik **24**, (2014).

[11] F.A. Olsson LE, Ericsson A, Mattsson S, "MR imaging of absorbed dose distributions for radiotherapy using ferrous sulphate gels," Physics in Medicine and Biology **35**, 1623-31 **(**1990).

[12] R. G. Kelly, K.J. Jordan, J. J. Battista, "Optical CT reconstruction of 3D dose distributions using the ferrous–benzoic–xylenol (FBX) gel dosimeter," Medical Physics **25**, 1741-50 (1998).

[13] L.J. Schreiner, "Review of Fricke gel dosimeters," Journal of Physics: Conference Series **3**, 9-21 (2004).

[14] M. J. Maryanski, G.S. Ibbott, P. Eastman, R. J. Schulz, J. C. Gore, "Radiation therapy dosimetry using magnetic resonance imaging of polymer gels," Medical Physics **23**, 699-705 (1996).

[15] G. S. Ibbott, M. J. Maryanski, P. Eastman, S. D. Holcomb, Y. Zhang, R. G. Avison, M. Sanders, J. C. Gore, "Three-dimensional visualization and measurement of conformal dose distributions using magnetic resonance imaging of bang polymer gel dosimeters," International Journal of Radiation Oncology, Biology, Physics **38**, 1097-1103 (1997).

[16] M. Oldham, "3D dosimetry by optical-CT scanning," Journal of physics. Conference series **56**, 58-71 (2006).

[17] J. Adamovics, M. J. Maryanski, "Characterisation of PRESAGE: A new 3-D radiochromic solid polymer dosemeter for ionising radiation," Radiation Protection Dosimetry **120**, 107-112 (2006).

[18] H.S. Sakhalkar, J. Adamovics, G. Ibbott, M. Oldham, "A comprehensive evaluation of the PRESAGE/optical-CT 3D dosimetry system," Medical Physics **36**, 71 (2009).

[19] H.R. Gorjiara T, Kuncic Z, Adamovics J, Bosi S, Kim JH, Baldock C, "Investigation of radiological properties and water equivalency of PRESAGE dosimeters," Medical Physics **38**, 2265-2274 (2011).

[20] T. Juang, J. Newton, M. Niebanck, R. Benning, J. Adamovics, M. Oldham, "Customising PRESAGE for diverse applications," Journal of Physics: Conference Series **444 (**2013).

[21] T. Juang, S. Das, J. Adamovics, R. Benning, M. Oldham, "On the need for comprehensive validation of deformable image registration, investigated with a novel 3-dimensional deformable dosimeter," International Journal of Radiation Oncology, Biology, Physics **87**, 414-421 (2013).

[22] A. Molineu, N. Hernandez, T. Nguyen, G. Ibbott, D. Followill, "Credentialing results from IMRT irradiations of an anthropomorphic head and neck phantom," Medical Physics **40**, (2013).

[23] J. Newton, M. Oldham, A. Thomas, Y. Li, J. Adamovics, D.G. Kirsch, S. Das, "Commissioning a small-field biological irradiator using point, 2D, and 3D dosimetry techniques," Medical Physics **38**, 6754-6762 (2011).

[24] L. J. Rankine, J. Newton, S. T. Bache, S. Das, J. Adamovics, D. G. Kirsch, M. Oldham, "Investigating end-to-end accuracy of image guided radiation treatment

delivery using a micro-irradiator," Physics in Medicine and Biology **58**, 7791-7801 (2013).

[25] J.C. Gore, M. Ranade, M.J. Maryanski, R.J. Schulz, "Radiation dose distributions in three dimensions from tomographic optical density scanning of polymer gels: I. Development of an optical scanner," Physics in Medicine and Biology **41**, 2695-2704 (1996).

[26] A. Thomas, M. Oldham, "Fast, large field-of-view, telecentric optical-CT scanning system for 3D radiochromic dosimetry," Journal of Physics: Conference Series **250**, 1-5 (2010).

[27] A. Thomas, J. Newton, J. Adamovics, M. Oldham, "Commissioning and benchmarking a 3D dosimetry system for clinical use," Medical Physics **38**, 4846-57 (2011).

[28] M. Matinfar, O. Gray, I. Iordachita, C. Kennedy, E. Ford, J. Wong, R.H. Taylor, P. Kazanzides, "Small animal radiation research platform: imaging, mechanics, control and calibration," Medical image computing and computer-assisted intervention **10**, 926-934 (2007).

[29] E. Doney, L.A. Krumdick, J.M. Diener, C.A. Wathen, S.E. Chapman, B. Stamile, J.E. Scott, M.J. Ravosa, T. Van Avermaete, W.M. Leevy, "3D printing of preclinical X-ray computed tomographic data sets," Journal of Visualized Experiments : JoVE **73**, (2013).

[30] A. Fedorov, R. Beichel, J. Kalpathy-Cramer, J. Finet, J. C. Fillion-Robin, S. Pujol, C. Bauer, D. Jennings, F. Fennessy, M. Sonka, J. Buatti, S. R. Aylward, J. V. Miller, S. Pieper, R. Kikinis, "3D Slicer as an Image Computing Platform for the Quantitative Imaging Network," Magnetic Resononce Imaging **30**, 1323-1341 (2012).

[31] "Somos Protogen 18420 Material Data Safety Sheet." www.dsmsomos.com (Accessed 2013)

[32] I. Stanton, M. Belley, G. Nguyen, A. Rodrigues, Y. Li, D. Kirsch, T. Yoshizumi, M. Therien, "Europium- and Lithium-Doped Yttrium Oxide Nanocrystals that Provide a Linear Emissive Response with X-ray Radiation Exposure," Nanoscale (Epub ahead of print, 2014).

[33] M. Dewhirst, G. Palmer, A. Fontanella, M. Boss, "Biological Considerations for Failure to Achieve Full Thermal Ablation", presented at the STM Spring Conference, Washington, DC, 2013 (unpublished).

[34] A. Thomas, M. Pierquet, K. Jordan, M. Oldham, "A method to correct for spectral artifacts in optical-CT dosimetry", Physics in Medicine and Biology **56**, 3403-3416 (2011).

[35] M. K. Boss, J. A. Somarelli, M.A. Garcia-Clanco, M.W. Dewhirst, "Radiation induces epithelial-mesenchymal transition in an in vitro mammary carcinoma tumor model", presented at the DCI Scientific Retreat, Durham, NC, 2013 (unpublished).

[36] S. Doran, D. N. Yatigammana, "Eliminating the need for refractive index matching in optical CT scanners for radiotherapy dosimetry: I. Concept and simulations," Physics in Medicine and Biology **57**, 665-83 (2012).

[37] L. Rankine, M. Oldham, "On the feasibility of optical-CT imaging in media of different refractive index," Medical Physics **40**, (2013).